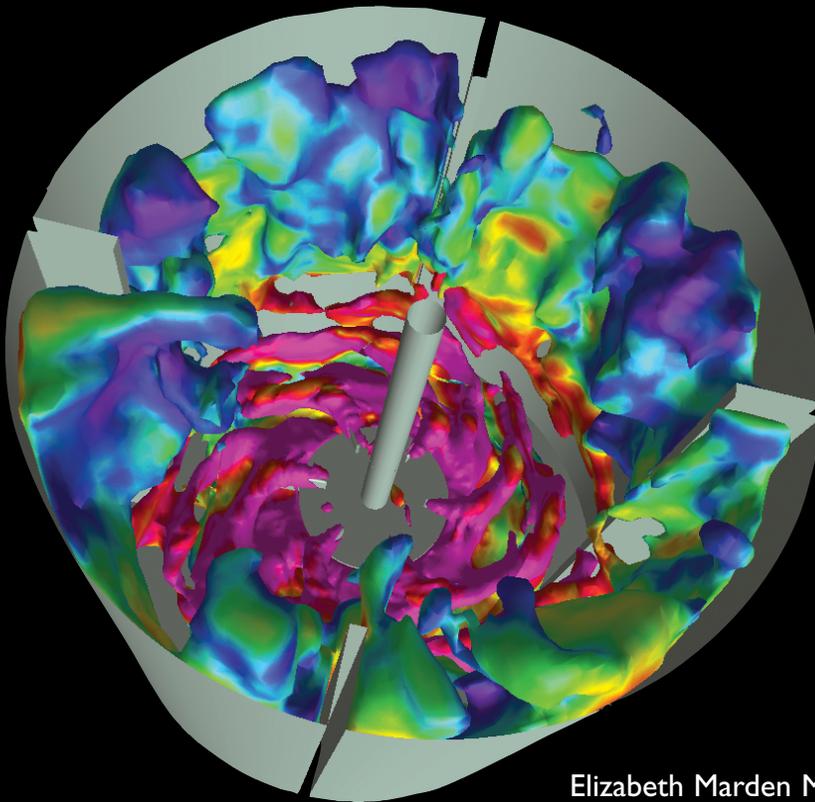# Computational Fluid Mixing

Elizabeth Marden Marshall
André Bakker

COMPUTATIONAL
FLUID MIXING

COMPUTATIONAL FLUID MIXING

Elizabeth Marden Marshall and André Bakker

ACKNOWLEDGEMENTS

THE AUTHORS

Elizabeth Marden Marshall is the technical archive manager at Fluent Inc. in Lebanon, New Hampshire. She has been with Fluent Inc. for more than ten years. She has extensive experience in a wide range of industrial applications, with special focus in the chemical process and mixing areas. She holds a Bachelor degree in mathematics from St. Lawrence University and a Ph.D. in physics from Dartmouth College, and is a member of AIChE.

André Bakker is the regional consulting manager at Fluent Inc. in Lebanon, New Hampshire. Bakker is an internationally recognized expert in the field of industrial mixing and CFD modeling of chemical engineering applications. His specialization includes experimental and computational fluid mixing. He holds engineering and doctorate degrees from Delft University of Technology in the Netherlands, both in applied physics. He has coauthored more than 50 technical articles and presentations on fluid dynamics and mixing, and is a member of AIChE. He also maintains a personal webpage on computational fluid mixing at www.bakker.org/cfm/.

TABLE OF CONTENTS

FOREWORD

by John M. Smith
Professor of Process Engineering
University of Surrey,
Guildford, Surrey, UK

Mixing is an ancient art, which, despite being practiced for thousands of years, has often been taken for granted. It has come a long way during the past few centuries, and in particular, during the past few decades. Many of the recent advances are the result of computerized measurement and simulation techniques that are now ubiquitous in laboratories throughout the world. Despite the proliferation of these modern methods, there is still much to be learned from the scientists and engineers of the past, whose mechanical ingenuity and wisdom continue to deserve our utmost respect.

i

COMPUTATIONAL FLUID MIXING

The only records of early equipment deal with particular difficulties and, prior to the twentieth century, there is little information about the evolution of the technology. The classic book "De Re Metallica" (The Kingdom of Metals), written by Georgius Agricola c. 1550, and translated and published as a Dover Reprint in 1950, suggests that even in the sixteenth century manual mixing was being supplemented by mechanical agitation, particularly for continuous processes. The engravings illustrating Agricola's book include one showing a four-stage suspension and extraction train followed by a laundering cascade. This is a three phase mixing operation - the plant is using mercury extraction on an aqueous suspension of gold bearing sand. The picture shows the six bladed paddles - remarkably similar to many in use today - driven by gearing that allows some vertical movement of the shafts in the contacting vessels.

The distinctive design of the horizontal axis impellers, used to prevent buildup and blockage in the launders, can also be seen.

Another interesting archive of traditional practice is Andrew Ure's "Encyclopaedia of Arts Minerals and Mines", published in London in 1843 and reprinted by Appleton & Co. of Philadelphia in 1851. Two engravings from this source illustrate large scale mixers that make use of the mechanical advantage of (true) horse power and geared drives.

The horse-driven mixer is a pug mill preparing clay for brick making. The illustration also shows one half of the machinery used for filling the brick molds. The mill partially (perhaps totally) replaced a process in which the laborers were required to stamp around in the clay as they separated and removed stones and other contaminants. The mixing vessel, which appears to be about eight feet high and five feet in diameter, has an agitator with about six inclined paddle impellers. Since there is literally one horsepower input, there is a specific energy consumption of about 6 HP/1000 US gallons, a value that is perhaps not unreasonable for this rather difficult mixing operation.

A planetary mixer, described in the same source, has an agitator shaft that rotates approximately seventeen times during each circuit of the vessel. The mixer was developed for the mashing stage of a brewing process. Gentle agitation, preferred during the initial wetting of the malt, was followed by more vigorous mixing to maintain the homogeneity of the two-phase mixture. The

complex gearing allowed the speed of the mixer to be selected as required. The planetary motion of the relatively small diameter, up-pumping agitator sweeps out the whole vessel volume without imposing unreasonable stresses on the impeller or its shaft. It is clear that the complex time dependent flow in this mixer configuration would be a real challenge to computational modeling!
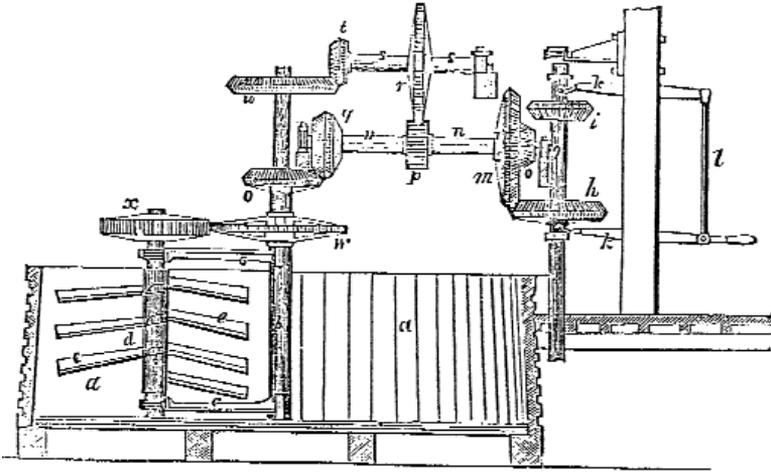
During the second half of the twentieth century, the evolution of mixing equipment and theory has grown dramatically. Experimental techniques have allowed engineers to better understand the action of impellers operating in many regimes, and the advent of computational fluid dynamics has enhanced this knowledge. The conversion of some engineers to believers in computational methods has taken some time, but their cautious approach is not new. For years scientists have had to adopt ways to grapple with new concepts and ideas. For Lord Kelvin[1], this meant developing mathematical models to explain his observations:

"I am never content until I have constructed a mathematical model of the subject I am studying. If I succeed in making one, I understand; otherwise I do not."

Other modern-day scientists take a more practical point of view. These folks view computational methods as an inexpensive way to experiment with new ideas, test them for feasibility, and deliberately make mistakes to examine the consequences. According to John McLeod and John Osborn[2],

"In real life mistakes are inevitable. Computer simulation however makes it economically possible to make mistakes on purpose. If you are astute therefore, you can learn much more than they cost. Furthermore if you are at all discreet, no one but you need ever know you made a mistake."

Despite the fact that the proper place for CFD in the field of mixing is still not well defined in the minds of some, it has been proven to be an invaluable source of insight for many others. In the chapters of this book, the authors carefully review the basics of this technology, and illustrate how it can be applied to mixing applications of many varieties. A few open questions remain, particularly with multiphase systems. The present models for bubble or droplet coalescence dynamics or of the mechanisms of particle pickup from the base of a vessel are immature. However, progress is rapid and we can look forward with confidence to the development of better simulations of these and other difficult aspects of mixing operations.

COMPUTATIONAL FLUID MIXING

[1]Kelvin, William Thomson, Baron, 1824-1907, Notes of lectures on molecular dynamics and the wave theory of light. Delivered at the Johns Hopkins University, Baltimore, by Sir William Thomson Kelvin, Stenographically reported by A. S. Hathaway, 1884.

[2]John McLeod and John Osborn, Natural Automata and Useful Simulations, ed. P H Pattee et al. McMillan, (1966).

I

INTRODUCTION

Mixing processes can be based on a number of mechanisms, from agitation to sparging to static flow manipulation. Agitation in a stirred tank is one of the most common operations, yet presents one of the greatest challenges in the area of computer simulation. Stirred tanks typically contain an impeller mounted on a shaft, and optionally can contain baffles and other internals such as spargers, coils, and draft tubes. Modeling a stirred tank using computational fluid dynamics (CFD) requires consideration of many aspects of the process. First, any computational model requires that the domain of interest, in this case the volume occupied by the fluid inside the vessel, be described by a computational grid, a collection of small sub-domains or cells. It is in these cells that problem-specific variables are computed and stored. The computational grid must fit the contours of the vessel and its internals, even if the components are geometrically complex. Second, the motion of the impeller in the tank must be treated in a special way, especially if the tank contains baffles or other internals. The special treatment employed impacts both the construction of the computational grid as well as the solution method used to numerically obtain the flow field. In this book,

the process of modeling the flow inside a stirred tank is examined, and these special considerations are discussed at length.

The material presented in subsequent sections is summarized below.

Chapter II: Introduction to Computational Fluid Dynamics
Chapter III: Introduction to Numerical Methods
Chapter IV: Modeling a Stirred Tank with Experimental Data
Chapter V: Modeling a Stirred Tank Using Actual Impeller
               Geometry
Chapter VI: Evaluating Mixing from Flow Field Results
Chapter VII: Application Examples
Chapter VIII: Closing Remarks

In Chapter II, an introduction to the field of computational fluid dynamics is given, with an emphasis on the fundamental equations that are used to describe processes that are common in mixing applications. An overview of the numerical methods used to solve these equations is presented in Chapter III.

Numerical simulations of stirred tanks are normally done in either two or three dimensions. In 2D simulations, the geometry and flow field are assumed to be axisymmetric, or independent of the angular dimension. The solution domain extends from the axis of the vessel out to the vessel wall. Approximations are required for elements that do have angular dependence, such as the impellers and baffles. These approximate methods are discussed in Chapter IV. In 3D simulations, the impellers, baffles, and other internals can be modeled using their exact geometry. The challenge in these simulations is to incorporate the motion of

the impeller in the presence of the stationary tank and internals. Methods for performing 3D simulations are discussed in Chapter V. Chapter VI illustrates how CFD results can be interpreted for mixing analysis. Several application examples are presented in Chapter VII, and closing remarks, including a review of some of the common pitfalls to success, are given in Chapter VIII.

Figure 1.1 shows the outline of a simple baffled stirred tank containing a Rushton turbine on a centrally mounted shaft. The tank has diameter T. The impeller has diameter D, and is located a distance C off the bottom of the tank. These symbols will be used throughout the book. In addition, references will be made to the computational grid that is necessary for computing a numerical solution for the flow field in a stirred tank when the impeller is operational. This grid can take on many forms, as is discussed in Chapter III. One example of a computational grid for the vessel of Figure 1.1 is shown in Figure 1.2.
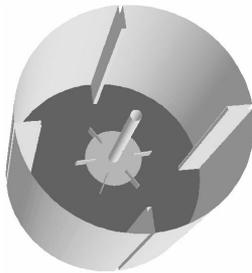
Figure 1.1
Simple vessel showing a Rushton turbine on a central shaft and baffles.
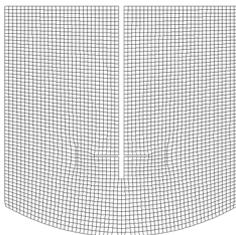
Figure 1.2
An example of a computational grid that can be used for the solution of the flow field in this vessel.

COMPUTATIONAL FLUID MIXING

II

INTRODUCTION TO COMPUTATIONAL FLUID DYNAMICS

Computational fluid dynamics, or CFD, is the numerical simulation of fluid motion. While the motion of fluids in mixing is an obvious application of CFD, there are hundreds of others, ranging from blood flow through arteries, to supersonic flow over an airfoil, to the extrusion of rubber in the manufacture of automotive parts. Numerous models and solution techniques have been developed over the years to help describe a wide variety of fluid motion. In this section, the fundamental equations for fluid flow are presented as follows:

Section 2.1: Conservation equations (for fluid flow, turbulence, chemical species transport, and heat transfer)

Section 2.2: Auxiliary models (for chemical reaction, multi-phase flow, and non-Newtonian viscosity)

While the primary focus is on specific models that are relevant to the analysis of mixing processes, a number of advanced models for more complex flows are also discussed.

COMPUTATIONAL FLUID MIXING

2.1 Conservation Equations

If a small volume, or element of fluid in motion is considered, two changes to the element will most likely take place. First, the fluid element will translate and possibly rotate in space, and second, it will become distorted, either by a simple stretching along one or more axes, or by an angular distortion that causes it to change shape. The process of translation is often referred to as convection, while the process of distortion is related to the presence of gradients in the velocity field and a process called diffusion. In the simplest case, these processes govern the evolution of the fluid from one state to another. In more complicated systems, sources can also be present that give rise to additional changes in the fluid. Many more phenomena can also contribute to the way a fluid element changes with time. Heat can cause a gas to expand, and chemical reactions can cause the viscosity to change, for example. Many of the processes such as those that are involved in the description of generalized fluid motion are described by a set of conservation, or transport equations. These equations track, over time, changes in the fluid that result from convection, diffusion, and sources or sinks of the conserved or transported quantity. Furthermore, these equations are coupled, meaning that changes in one variable (say, the temperature) can give rise to changes in other variables (say, the pressure). The equations discussed below describe many of these coupled phenomena, with an emphasis on those processes that are typical in mixing applications.

2.1.1 Continuity

The continuity equation is a statement of conservation of mass. To understand its origin, consider the flow of a fluid of density ρ through the six faces of a rectangular block, as shown in Figure 2.
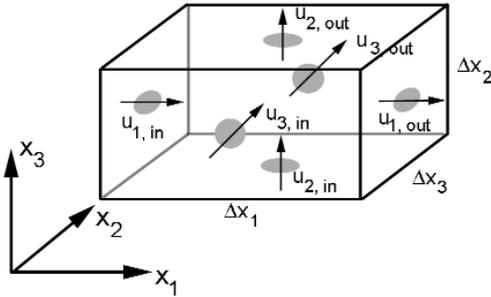
Figure 2
A rectangular volume with inflow and outflow can be used to illustrate a conservation equation.

The block has sides of length Δx_1, Δx_2, and Δx_3 and velocity components u_1, u_2, and u_3 in each of the three coordinate directions. To ensure conservation of mass, the sum of the mass flowing through all six faces must be zero.

$$\rho\left(U_{1,out} - U_{1,in}\right)\left(\Delta x_2 \Delta x_3\right) + \rho\left(U_{2,out} - U_{2,in}\right)\left(\Delta x_1 \Delta x_3\right) + \rho\left(U_{3,out} - U_{3,in}\right)\left(\Delta x_1 \Delta x_2\right) = 0 \quad (1)$$

Dividing through by $(\Delta x_1\, \Delta x_2\, \Delta x_3)$ the equation can be written as:

$$\rho \frac{\Delta U_1}{\Delta x_1} + \rho \frac{\Delta U_2}{\Delta x_2} + \rho \frac{\Delta U_3}{\Delta x_3} = 0 \tag{2}$$

or, in differential form:

$$\rho \frac{\partial U_1}{\partial x_1} + \rho \frac{\partial U_2}{\partial x_2} + \rho \frac{\partial U_3}{\partial x_3} = 0 \tag{3}$$

A more compact way to write Eq. (3) is through the use of Einstein notation:

$$\rho \frac{\partial U_i}{\partial x_i} = 0 \tag{4}$$

With this notation, whenever repeated indices occur in a term, the assumption is that there is a sum over all indices. Here, and elsewhere in this book, U_i is the ith component of the fluid velocity,

7

and partial derivatives with respect to x_i are assumed to correspond to one of the three coordinate directions. For more general cases, the density can vary in time and in space, and the continuity equation takes on the more familiar form:

$$\frac{\partial \rho}{\partial t} + \frac{\partial}{\partial x_i}(\rho U_i) = 0 \qquad (5)$$

2.1.2 Momentum

The momentum equation is a statement of conservation of momentum in each of the three component directions. The three momentum equations are collectively called the Navier-Stokes equations. In addition to momentum transport by convection and diffusion, several momentum sources are also involved.

$$\frac{\partial(\rho U_i)}{\partial t} + \frac{\partial}{\partial x_j}\left(\rho U_i U_j\right) = -\frac{\partial p}{\partial x_i} + \frac{\partial}{\partial x_j}\left[\mu\left(\frac{\partial U_i}{\partial x_j} + \frac{\partial U_j}{\partial x_i} - \frac{2}{3}\frac{\partial U_k}{\partial x_k}\delta_{ij}\right)\right] + \rho g_i + F_i \qquad (6)$$

In Eq. (6), the convection terms are on the left. The terms on the right hand side are the pressure gradient, a source term; the divergence of the stress tensor, which is responsible for the diffusion of momentum; the gravitational force, another source term; and other generalized forces (source terms), respectively.

2.1.3 Turbulence

A number of dimensionless parameters have been developed for the study of fluid dynamics that are used to categorize different flow regimes. These parameters, or numbers, are used to classify fluids as well as flow characteristics. One of the most common of these is the Reynolds number, defined as the ratio of inertial forces, or those that give rise to motion of the fluid, to frictional forces, or those that tend to slow the fluid down. In geometrically similar domains, two fluids with the same Reynolds

number should behave in the same manner. For simple pipe flow, the Reynolds number is defined as

$$\text{Re} = \frac{\rho U d}{\mu} \tag{7}$$

where ρ is the fluid density, U is the axial velocity in the pipe, d is the pipe diameter, and μ is the molecular, or dynamic viscosity of the fluid. For mixing tanks, a modified definition is used:

$$\text{Re} = \frac{N D^2 \rho}{\mu} \tag{8}$$

where N is the impeller speed, in revolutions/sec, and D is the impeller diameter. Based on the value of the Reynolds number, flows fall into either the laminar regime, with small Reynolds numbers, or the turbulent regime, with high Reynolds numbers. The transition between laminar and turbulent regimes occurs throughout a range of Reynolds numbers, rather than at a single value. For pipe flow, transition occurs in the vicinity of Re = 2000, while in mixing tanks, it is usually different, occurring somewhere between Re = 50 and 5000. In the turbulent regime, fluctuations in the mean velocity and other variables occur, and their effect needs to be incorporated into the CFD model in order for the model to be able to provide meaningful results. This is done through the use of a turbulence model.

Several methods are available for including turbulence in the Navier-Stokes equations. Most of these involve a process of time-averaging the conservation equations. When turbulence is included, the transported quantity, say velocity, is assumed to be the sum of an equilibrium and a fluctuating component, $U_i + u_i'$. After time-averaging over many cycles of the fluctuation, terms

containing factors of the fluctuating component average to zero. The only term that remains positive definite is one containing the product of two fluctuating terms. The remaining terms are identical to those in Eq. (6) above. Thus the so-called Reynolds-Averaged Navier-Stokes, or RANS equation for momentum is:

$$\frac{\partial(\rho U_i)}{\partial t} + \frac{\partial}{\partial x_j}(\rho U_i U_j) = -\frac{\partial p}{\partial x_i} + \frac{\partial}{\partial x_j}\left[\mu\left(\frac{\partial U_i}{\partial x_j} + \frac{\partial U_j}{\partial x_i} - \frac{2}{3}\frac{\partial U_k}{\partial x_k}\delta_{ij}\right)\right]$$
$$+ \frac{\partial}{\partial x_j}\left(-\rho\overline{u_i'u_j'}\right) + \rho g_i + F_i \tag{9}$$

The new terms involving $\overline{u_i'u_j'}$ are called the Reynolds stresses. The overbar indicates that these terms represent time-averaged values. Reynolds stresses contribute new unknowns to the RANS equations, and need to be related to the other variables. A variety of turbulence models are available for this purpose.

The Boussinesq Hypothesis

The Boussinesq hypothesis makes the assumption that the Reynolds stresses can be expressed in terms of mean velocity gradients. The statement of the hypothesis below, shows the introduction of a new constant that is dimensionally equivalent to viscosity:

$$\rho\overline{u_i'u_j'} = \frac{2}{3}\rho k \delta_{ij} + \left(\mu_t\left[\frac{\partial U_i}{\partial x_j} + \frac{\partial U_j}{\partial x_i}\right]\right) \tag{10}$$

The new constant, μ_t, is the turbulent, or eddy viscosity. It can be seen that when Eq. (10) is substituted into Eq. (9), the terms containing the partial derivatives can be combined and a new quantity, the effective viscosity, can be introduced:

$$\mu_{eff} = \mu + \mu_t \tag{11}$$

The hypothesis also introduces another term involving a new variable, *k*, the kinetic energy of turbulence. This quantity is defined in terms of the velocity fluctuations *u', v',* and *w'* in each of the three coordinate directions:

$$k = \frac{1}{2}\left(\overline{u'^2} + \overline{v'^2} + \overline{w'^2}\right) \tag{12}$$

It is the job of the turbulence model to compute the Reynolds stresses for substitution into Eq. (9). In some cases, this is done by computing the parameters k and μ_t (or k and μ_{eff}) for substitution into Eq. (10) and ultimately, Eq. (9). All turbulence models use some level of approximation to accomplish this goal, and it is the nature of the flow conditions in each specific application that determines which set of approximations is acceptable for use. A brief summary of some of the popular turbulence models in use today for industrial applications is given below.

The k-ε Model

The k-ε model is one of a family of two-equation models, for which two additional transport equations must be solved in order to compute the Reynolds stresses. (Zero- and one-equation models also exist, but are not commonly used in mixing applications.) It is a robust model, meaning that it is computationally stable, even in the presence of other, more complex physics. It is applicable to a wide variety of turbulent flows, and has served the fluid modeling community for many years. It is semi-empirical, based in large part on observations of mostly high Reynolds number flows. The two transport equations that need to be solved for this model are for the kinetic energy of turbulence, *k*, and the rate of dissipation of turbulence, *ε*:

$$\frac{\partial(\rho k)}{\partial t} + \frac{\partial}{\partial x_i}(\rho U_i k) = \frac{\partial}{\partial x_i}\left(\mu + \frac{\mu_t}{\sigma_k}\right)\frac{\partial k}{\partial x_i} + G_k - \rho\varepsilon \qquad (13)$$

$$\frac{\partial(\rho\varepsilon)}{\partial t} + \frac{\partial}{\partial x_i}(\rho U_i \varepsilon) = \frac{\partial}{\partial x_i}\left(\mu + \frac{\mu_t}{\sigma_\varepsilon}\right)\frac{\partial\varepsilon}{\partial x_i} + C_1\frac{\varepsilon}{k}G_k + C_2\rho\frac{\varepsilon^2}{k} \qquad (14)$$

The quantities C_1, C_2, σ_k, and σ_ε are empirical constants. The quantity G_k appearing in both equations is a generation term for turbulence. It contains products of velocity gradients, and also depends on the turbulent viscosity:

$$G_k = \mu_t\left(\frac{\partial U_i}{\partial x_j} + \frac{\partial U_j}{\partial x_i}\right)\frac{\partial U_j}{\partial x_i} \qquad (15)$$

Other source terms can be added to Equations (13) and (14) to include other physical effects such as swirl, buoyancy or compressibility, for example. The turbulent viscosity is derived from both k and ε, and involves a constant taken from experimental data, C_μ, which has a value of 0.09:

$$\mu_t = \rho C_\mu\frac{k^2}{\varepsilon} \qquad (16)$$

To summarize the solution process for the k-ε model, transport equations are solved for the turbulent kinetic energy and dissipation rate. The solutions for k and ε are used to compute the turbulent viscosity, μ_t. Using the results for μ_t and k, the Reynolds stresses can be computed for substitution into the momentum equations. Once the momentum equations have been solved, the new velocity components are used to update the turbulence generation term, G_k, and the process is repeated.

The RNG k-ε Model

The RNG model (Yakhot, 1986) was developed in response to the empirical nature of the standard k-ε model. Rather than being based on observed fluid behavior, it is derived using statistical methods used in the field of renormalization group (RNG) theory. It is similar in form to the standard k-ε model, but contains modifications in the dissipation equation to better describe flows with regions of high strain, such as the flow around a bend or reattachment following a recirculation zone. In addition, a differential equation is solved for the turbulent viscosity. When the solution of this differential equation is evaluated in the high Reynolds number limit, Eq. (16) is returned with a coefficient, C_μ, of 0.0845, within 7% of the empirical value of 0.09. While the RNG model works well for high Reynolds number flows, it also works well for transitional flows, where the Reynolds number is in the low turbulent range.

The Realizable k-ε Model

The realizable k-ε model (Shih, 1995) is a fairly recent addition to the family of two-equation models. It differs from the standard k-ε model in two ways. First, the turbulent viscosity is computed in a different manner, making use of Eq. (16), but using a variable for the quantity C_μ. This is motivated by the fact that in the limit of highly strained flow, some of the normal Reynolds stresses $\overline{u_i^2}$, can become negative in the k-ε formulation, which is unphysical, or unrealizable. The variable form of the constant C_μ is a function of the local strain rate and rotation of the fluid, and is designed to prevent unphysical values of the normal stresses from developing.

COMPUTATIONAL FLUID MIXING

The second difference is that the realizable k-ε model uses different source and sink terms in the transport equation for eddy dissipation. The resulting equation is considerably different from the one used for both the standard and RNG k-ε models. The modified prediction of ε, along with the modified calculation for μ_t, make this turbulence model superior to the other k-ε models for a number of applications. In particular, the model does better in predicting the spreading rate of round jets, such as those emitted from a rotating impeller blade.

The RSM Model

The Reynolds stress model (RSM) does not use the Boussinesq hypothesis. Rather than assume that the turbulent viscosity is isotropic, having one value, as is done in the k-ε model, the Reynolds stress model computes the stresses, $\overline{u_i' u_j'}$ individually. For 2D models, this amounts to four additional transport equations. For 3D models, six additional transport equations are required. Along with the transport equation for ε, which must also be solved in the RSM model, the full effect of turbulence can be represented in the momentum equations with greater accuracy than can be obtained from the k-ε models. Flows for which the assumption of isotropic turbulent viscosity breaks down include those with high swirl, rapid changes in strain rate, or substantial streamline curvature. As computer power and speed have increased during the past several years, the use of the Reynolds stress turbulence model has become more widespread, giving rise to improved accuracy over other RANS-based turbulence models when compared to experimental results for a number of applications, such as the flow in unbaffled stirred vessels.

The LES Model

A fairly recent entry to the group of commercially available turbulence models is the large eddy simulation, or LES model. This approach recognizes that turbulent eddies occur on many scales in a flow field. Large eddies are often sized according to the extents of the physical domain. Small eddies, however, are assumed to have similar properties and behavior for all problem domains, independent of their overall size or purpose. With the LES model, the continuity and momentum equations are filtered prior to being solved in a transient fashion. The filtering process isolates the medium- and large-scale eddies from those that are smaller than a typical cell size. The effects of the small eddies are included in the filtered equations through the use of a sub-grid-scale model. The transient simulation is then free to capture the random fluctuations that develop on the medium and large scales. Despite the fact that a transient simulation is needed for this turbulence model, it has proven to be worth the effort. Simulations to date have successfully predicted unstable behavior in jets, flames, and both static and stirred tank mixers. See, for example, Section 7.11, where LES is used to simulate the flow in an HEV static mixer.

An overview of the turbulence models discussed in this section, including the primary advantages and disadvantages of each, is provided in Table 1.

Table 1

Summary of turbulence models

Turbulence Model	Description, Advantages, and Disadvantages
Standard k-ε	The most widely used model, it is robust, economical, and has served the engineering community well for many years. Its main advantages are a rapid, stable calculation, and reasonable results for many flows, especially those with high Reynolds number. It is not recommended for highly swirling flows, round jets, or for flows with strong flow separation.
RNG k-ε	A modified version of the k-ε model, this model yields improved results for swirling flows and flow separation. It is not well suited for round jets, and is not as stable as the standard k-ε model.
Realizable k-ε	Another modified version of the k-ε model, the realizable k-ε model correctly predicts the flow in round jets, and is also well suited for swirling flows and flows involving separation.
RSM	The full Reynolds stress model provides good predictions for all types of flows, including swirl, separation, and round and planar jets. Because it solves transport equations for the Reynolds stresses directly, longer calculation times are required than for the k-ε models.
LES	Large eddy simulation is a transient formulation that provides excellent results for all flow systems. It solves the Navier-Stokes equations for large scale turbulent fluctuations and models only the small scale fluctuations (smaller than a computational cell). Because it is a transient formulation, the required computational resources are considerably larger than those required for the RSM and k-ε style models. In addition, a finer grid is needed to gain the maximum benefit from the model, and to accurately capture the turbulence in the smallest, sub-grid scale eddies.

2.1.4 Species

The species equation is a statement of conservation of a single species. Multiple species equations can be used to represent fluids in a mixture with different physical properties. Solution of the species equations can predict how different fluids mix, but not how they will separate. Separation is the result of different

body forces acting on the fluids, such as gravity acting on fluids of different density. To model separation, separate momentum equations are required for each of the fluids so that the body forces can act on the fluids independently. (See Section 2.2.2). Species transport is nevertheless a very useful tool for predicting blending times or chemical reaction. For the species i', the conservation equation is for the mass fraction of that species, $m_{i'}$, and has the following form:

$$\frac{\partial(\rho m_{i'})}{\partial t} + \frac{\partial}{\partial x_i}(\rho U_i m_{i'}) = -\frac{\partial}{\partial x_i} J_{i',\,i} + R_{i'} + S_{i'} \tag{17}$$

In Equation (17), $J_{i',i}$ is the i component of the diffusion flux of species i' in the mixture. For laminar flows, $J_{i',i}$ is related to the diffusion coefficient for the species and local concentration gradients. For turbulent flows, $J_{i',i}$ also includes a turbulent diffusion term, which is a function of the turbulent Schmidt number. $R_{i'}$ is the rate at which the species is either consumed or produced in one or more reactions, and $S_{i'}$ is a general source term for species. The general source term can be used for non-reacting sources, such as the evaporated vapor from a heated droplet, for example. When two or more species are present, the sum of the mass fractions in each cell must add to 1.0. For this reason, if there are n species involved in a simulation, only n-1 species equations need to be solved. The mass fraction of the nth species can be computed from the required condition:

$$\sum_{i'}^{n} m_{i'} = 1.0 \tag{18}$$

More details about reacting flow are presented in Section 2.2.1.

2.1.5 Heat Transfer
Heat transfer is often expressed as an equation for the conserva-

tion of energy, typically in the form of static or total enthalpy. Heat can be generated (or extracted) through many mechanisms, such as wall heating (in a jacketed reactor), cooling through the use of coils, and chemical reaction. In addition, fluids of different temperatures may mix in a vessel and the time for the mixture to come to equilibrium may be of interest. The equation for conservation of energy (total enthalpy) is:

$$\frac{\partial(\rho E)}{\partial t} + \frac{\partial}{\partial x_i}(U_i(\rho E + p)) = \frac{\partial}{\partial x_i}\left(k_{eff}\frac{\partial T}{\partial x_i} - \sum_{j'}h_{j'}J_{j',i} + U_j(\tau_{ij})_{eff}\right) + S_h \quad (19)$$

In this equation, the energy, E, is related to the static enthalpy, h, through the following relationship involving the pressure, p, and velocity magnitude, U:

$$E = h - \frac{p}{\rho} + \frac{U^2}{2} \quad (20)$$

For incompressible flows with species mixing, the static enthalpy is defined in terms of the mass fractions, $m_{j'}$, and enthalpies, $h_{j'}$, of the individual species:

$$h = \sum_{j'}m_{j'}h_{j'} + \frac{p}{\rho} \quad (21)$$

The enthalpy for the individual species j' is a temperature-dependent function of the specific heat of that species:

$$h_{j'} = \int_{T,ref}^{T}c_{p,j'}dT \quad (22)$$

Once the enthalpy has been determined from the relationships shown above, the temperature can be extracted using Equation (22). This process is not straightforward because the temperature is the integrating variable. One technique for extracting the tem-

perature involves the construction of a look-up table at the start of the calculation, using the known or anticipated limits for the temperature range. This table can subsequently be used to obtain temperature values for corresponding enthalpies obtained at any time during the solution.

The first term on the right hand side of Eq. (19) represents heat transfer due to conduction, or the diffusion of heat, where the effective conductivity, k_{eff}, contains a correction for turbulent simulations. The second term represents heat transfer due to the diffusion of species, where $J_{j',i}$ is the diffusion flux defined in Section 2.1.4. The third term involves the stress tensor, a collection of velocity gradients, and represents heat loss through viscous dissipation. The fourth term is a general source term that can include heat sources due to reactions, radiation, or other processes.

2.2 Auxiliary Models

While a wide range of applications can be modeled using the basic transport equations described above, others involve more complex physics and require additional modeling capabilities. Some of these models are discussed below.

2.2.1 Chemical Reaction

Chemically reacting flows are those in which the chemical composition, properties, and temperature change as the result of a simple or complex chain of reactions in the fluid. Depending on the implementation, reacting flows can require the solution of multiple conservation equations for species, some of which describe reactants, and others of which describe products. To balance the mass transfer from one species to another, reaction

rates are used in each species conservation equation, and have as factors the molecular weights, concentrations, and stoichiometries for that species in all reactions.

Consider for example the single step, first order reaction: A + B → R, for which the reaction rate is given by:

$$R_i \propto \left(C_A C_B + \overline{c_A c_B} \right) \tag{23}$$

Here C_A and C_B (upper case) denote the mean molar concentrations of reactants A and B while c_A and c_B (lower case) denote the local concentration fluctuations that result from turbulence. When the species are perfectly mixed the second term on the right hand side, containing the correlation of the concentration fluctuations, will approach zero. If the species are not perfectly mixed, this term will be negative and will reduce the reaction rate. The estimation of this correlation term is not straightforward and numerous models are available (Hannon, 1992) for this purpose. Its presence suggests, however, that the reaction rate should incorporate not only the mean concentrations of the reactant species, but the turbulent fluctuations of the reactant species as well, since the latter gives an indication of the degree to which these species are mixed.

One popular method for computing the reaction rates as a function of both mean concentrations and turbulence levels is through the Magnussen model (Magnussen, 1976). Originally developed for combustion, it can also be used for liquid reactions by tuning some of the model parameters. The model consists of rates calculated by two primary means. An Arrhenius, or kinetic rate, $R_{K\_i',k}$, for species i' in reaction k, is governed by the local mean

species concentrations and temperature in the following manner:

$$R_{K\_i',k} = -v_{i',k} M_{i'} A_k T^{\beta_k} \exp\left(-\frac{E_k}{RT}\right) \prod_{j'=1}^{N} \left[C_{j'}\right]^{\eta_{j',k}} = K_{i',k} M_{i'} \prod_{j'=1}^{N} \left[C_{j'}\right]^{\eta_{j',k}} \quad (24)$$

This expression describes the rate at which species i' is con-sumed in reaction k. The constants A_k and E_k, the Arrhenius pre-exponential factor and activation energy, respectively, are adjust-ed for specific reactions, often as the result of experimental meas-urements. The stoichiometry for species i' in reaction k is rep-resented by the factor $v_{i',k}$, and is positive or negative, depending upon whether the species serves as a product or reactant. The molecular weight of the species i' appears as the factor $M_{i'}$. The temperature, T, appears in the exponential term and also as a fac-tor in the rate expression, with an optional exponent, β_k. Concentrations of other species, j', involved in the reaction, $[C_{j'}]$, appear as factors with optional exponents associated with each. Other factors and terms, not appearing in Eq. (24), can be added to include effects such as the presence of non-reacting species in the rate equation. Such so-called third-body reactions are typical of the effect of a catalyst on a reaction, for example. Many of the factors appearing in Eq. (24) are often collected into a single rate constant, $K_{i',k}$.

In addition to the Arrhenius rate, two mixing rates are computed that depend on the local turbulent kinetic energy and dissipation rate. One rate, $R_{M1,i',k}$, involves the mass fraction of the reactant in reaction k, m_R, that returns the smallest rate:

$$R_{M1,i',k} = v_{i',k} M_{i'} A\rho \frac{\varepsilon}{k} \frac{m_R}{v_{R,k} M_R} \quad (25)$$

where the subscript R refers only to the reactant species, $i' = R$.

COMPUTATIONAL FLUID MIXING

The other mixing rate, $R_{M2,i',k}$, involves the sum over product species mass fractions, m_P:

$$R_{M2,i',k} = v_{i',k} M_{i'} AB\rho \frac{\varepsilon}{k} \frac{\sum_P m_P}{\sum_{j'}^N v'_{j',k} M_{j'}}$$

(26)

In the mixing rate expressions, the values 4.0 and 0.5 are often used for the constants A and B, respectively, when the model is used for gaseous combustion. These values can be adjusted, however, for different types of reactions, such as those involving liquids.

After the rates in Equations (24), (25), and (26) are computed, the smallest, or slowest, is used as a source term in the species transport equations for all species involved in any given reaction. The basic idea behind the Magnussen model is that in regions with high turbulence levels, the eddy lifetime, k/ε, is short, mixing is fast, and as a result the reaction rate is not limited by small scale mixing. In this limit, the kinetic rate usually has the smallest value. On the other hand, in regions with low turbulence levels, small scale mixing may be slow and limit the reaction rate. In this limit, the mixing rates are more important.

The Magnussen model was initially developed for simple, one-step or two-step reaction sets, in which all reaction rates are fast relative to the small scale mixing, even though it has found use for more complex systems. Recently, for more complex reaction sets, an extension of this model has been developed (Gran and Magnussen (1996)) called the Eddy-Dissipation-Concept (EDC) model. This model assumes that reaction occurs in small turbulent structures, called the fine scales. A volume fraction of the

small scales is calculated, which depends on the kinematic viscosity of the fluid, the eddy dissipation rate, and the turbulent kinetic energy. Reactions are assumed to occur in the fine turbulent structures, over a time scale that depends on the kinematic viscosity and the energy dissipation rate. A source term for each chemical species is then calculated that depends on the volume fraction of the fine scales, the time scale, and the difference in species concentrations between the fine scale structures and the surrounding fluid. This extension of the Magnussen model provides improved accuracy for complex, multi-step reaction sets in which not all reactions are fast relative to the rate at which small scale mixing occurs.

Numerous other reaction models exist that can be coupled to the CFD calculation. For example, a collection of reacting species can be described by a mixture fraction, which, under certain circumstances, is a conserved quantity. This so-called PDF modeling approach is based on the assumptions of infinitely fast reactions and chemical equilibrium at all times. The model takes its name from the probability density function method that is used to describe the turbulence-chemistry interaction in the model. Rather than solve conservation equations for multiple species, conservation equations for the mean and variance of the mixture fraction are solved. The variation in the mixture fraction is representative of fluctuations in the species concentrations. Thus while the kinetic rate expression uses time-averaged values for species mass fractions, the PDF model allows for fluctuations in these quantities. Auxiliary reaction calculations allow for the extraction of intermediate and product species as a function of the mixture fraction and temperature distributions in the final CFD solution. While this model has many benefits for gaseous

combustion systems, it is not the best choice for liquid reactions that are typical of mixing applications, where reaction rates can fall anywhere from very fast to very slow when compared to typical mixing rates.

Another reaction modeling approach incorporates the methodology used to describe micromixing, or mixing on the smallest scales (Fox, 1998; Hannon, 1992; Bourne, et al., 1981). In the context of a CFD calculation, micromixing is on a scale that is smaller than a typical computational cell. Macromixing, on the other hand, is responsible for large scale blending, and mesomixing is in between these limits. The identification of these mixing regimes is drawn from assumptions at the core of turbulence modeling theory, namely that turbulence energy is generated in large eddies within a domain, and cascades to successively smaller eddies before being dissipated at the smallest scales. This cascade of turbulence is associated with a cascade of mixing, from macromixing on the large scales, to mesomixing throughout the mid-scales, to micromixing on the sub-grid scales. One motivation for the interest in micromixing in liquid reactions is that micromixing must occur before reactions can take place. It therefore plays an important role when the reaction times are on the same order as the mixing times. Micromixing models typically use a mixture fraction approach, and use a PDF formulation for the turbulence-chemistry interaction. The micromixing models are incorporated through the calculation of the variance of the mixture fraction.

2.2.2 Multiphase Flows

When multiple fluids are involved in a flow field, representing them by multiple species equations only works if the fluids are

mixing and not separating. Any separation caused by the action of body forces, such as gravity or centrifugal force, can only be captured by treating the fluids with a multiphase model. When such a model is used, each of the fluids is assigned a separate set of properties, including density. Because different densities are used, forces of different magnitude can act on the fluids, enabling the prediction of separation. Five of the most popular multiphase models that are in wide use in commercial software today are described below.

Dispersed or Discrete Phase Model
The dispersed phase model uses the Navier-Stokes equations to describe a continuous fluid phase, and a Lagrangian particle tracking method to describe a dispersed phase consisting of particles, droplets, or bubbles. Heat, mass, and momentum exchange is permitted between the dispersed and fluid phases. Thus gas bubbles can rise in a liquid, sand particles can settle, and water droplets can evaporate or boil, releasing steam to a background of warm gas, for example. The model is widely used for coal and liquid fuel combustion, bubble columns, and gas spargers in stirred tanks. It is best when the dispersed phase does not exceed 10% by volume of the mixture in any region.

VOF Model
The volume of fluid, or VOF model is designed for two or more immiscible fluids. Because the fluids do not mix, each computational cell is filled with either purely one fluid, purely another fluid, or the interface between two (or more) fluids. Because of this unique set of conditions, only a single set of Navier-Stokes equations is required. Each fluid is allowed to have a separate set of properties. The properties used are those of the fluid filling the

control volume. If the interface lies inside the control volume, special treatment is used to track its position and slope in both the control volume and neighboring cells as the calculation progresses. This model is used to track free surface flows or the rise of large bubbles in a liquid, for example.

Eulerian Multiphase Model
The Eulerian multiphase model is designed for systems containing two or more interpenetrating fluids. The fluids can be in the form of liquids, gases, or solids. Whereas the dispersed phase model works best for low volume fraction mixtures (<10%), the Eulerian multiphase model is general enough that any volume fraction of any phase is allowed. Separate sets of momentum and continuity equations are used to describe each fluid. Momentum transfer between the phases is incorporated through the use of exchange terms in the momentum equations. When heat and mass transfer between phases occurs, exchange terms are used in the energy and continuity equations as well. The volume fractions of the phases are tracked, with the condition that the sum of the volume fractions for all phases is identically 1.0 at all times in all control volumes. Separate equations can also be used for turbulence and species transport for each phase. While momentum, mass, heat, and species transfer between phases may be well understood, the same cannot be said for the coupling of the turbulence equations. This is an area that is currently undergoing active research at a number of institutions worldwide.

Eulerian Granular Multiphase Model
When the primary phase is a liquid or a gas and the secondary phase consists of solid particles, a modified form of the Eulerian multiphase model can be used. The Eulerian granular multiphase

(EGM) model uses kinetic theory to describe the behavior of the granular or particulate phase, which is different in many ways from that of a fluid phase. (See, for example, Ogawa *et al.* (1980), Ding *et al.* (1990), and Syamlal *et al.* (1993)). In particular, the viscosity of the granular phase undergoes a discontinuous change as the granular material transforms from a packed bed at rest to a fluid in motion, and this can only be captured by the special treatment at the heart of the EGM model. Also unique to the model is a solids pressure, which arises in part from inelastic collisions between particles. As is typical of a gas described by kinetic theory, a Maxwellian velocity distribution can be assumed for the granular phase. The width of this distribution, or spread in velocity fluctuations about the mean value, is related to the granular temperature, a parameter that can contribute to several other phenomena in granular multiphase flows. The maximum volume fraction that the granular phase can occupy is always less than 1.0 (typically 0.6), owing to the void that is always present between the particles. These and other issues are addressed by the EGM model, allowing it to simulate a wide array of granular flow applications, from solids suspension in stirred tanks to fluidized bed flow patterns to flow in a riser.

Algebraic Slip Mixture Model
As with the Eulerian multiphase model, the algebraic slip mixture, or ASM model is designed for use with two interpenetrating fluids. A full set of Navier-Stokes equations is solved for the primary fluid. Rather than solve a complete set for the secondary fluid, however, an algebraic equation for the slip velocity between the fluids is solved instead. The slip velocity is derived from the fluid properties and local flow conditions, and is used to compute the velocity of the secondary phase. The ASM model is

best when used for liquid-liquid or gas-liquid mixtures. It can also be used for lightly loaded granular mixtures, where the physics associated with the granular phase as it approaches the packing limit are not as important.

2.2.3 Non-Newtonian Viscosity

For Newtonian fluids, the viscosity often varies weakly with the temperature, by an amount that depends upon the temperature range in use. Many fluids do not fit this simple pattern, however, and have viscosities that also depend upon the shear rate in the fluid. The viscosity of these so-called non-Newtonian fluids can be described by one of a number of laws that involve the local shear rate of the fluid in one way or another. The dependence can be in the form of a power law (the shear rate raised to some power) and can involve a discontinuous transition after a minimum yield stress has been exceeded. In some cases, a fluid will transition from non-Newtonian to Newtonian behavior after a threshold stress has been exceeded. In general, shear-thinning fluids exhibit a drop in viscosity in regions of high shear, while shear-thickening fluids exhibit an increase in viscosity in these regions. For computational fluid dynamics, the consequence of non-Newtonian flow modeling is that the viscosity, a fluid property, becomes coupled to the fluid motion, making the equation set more difficult to solve if the viscosity is strongly varying within the limits of the flow field conditions.

Some non-Newtonian fluids are also described by a property called viscoelasticity. As for Newtonian fluids, these fluids deform when a shearing force is applied, but they have a partial memory of their state prior to the application of the force. Thus when the force is withdrawn, they return, to a greater or lesser

degree, to their previous state. Specialty CFD codes exist that have comprehensive models for both non-Newtonian and viscoelastic fluids. These codes are used for certain laminar mixing processes in stirred tanks and extruders.

COMPUTATIONAL FLUID MIXING

III

INTRODUCTION TO NUMERICAL METHODS

The differential equations presented in the previous section describe the continuous movement of a fluid in space and time. To be able to solve those equations numerically, all aspects of the process need to be discretized, or changed from a continuous to a discontinuous formulation. For example, the region where the fluid flows needs to be described by a series of connected control volumes, or computational cells. The equations themselves need to be written in an algebraic form. Advancement in time and space needs to be described by small, finite steps rather than the infinitesimal steps that are so familiar to students of calculus. All of these processes are collectively referred to as discretization. In this section, discretization of the domain, or grid generation, and discretization of the equations are described. A section on solution methods and one on parallel processing are also included:

Section 3.1: Discretization of the domain: grid generation
Section 3.2: Discretization of the equations
Section 3.3: Solution methods
Section 3.4: Parallel processing

31

3.1 Discretization of the Domain: Grid Generation

To break the domain into a set of discrete sub-domains, or computational cells, or control volumes, a grid is used. Also called a mesh, the grid can contain elements of many shapes and sizes. In 2D domains, for example, the elements are usually either quadrilaterals or triangles. In 3D domains, they can be tetrahedra (with four sides), prisms (five sides), pyramids (five sides) or hexahedra (six sides) (Figure 3).

Triangle   Tetrahedron   Hexahedron

Quad   Prism/Wedge   Pyramid
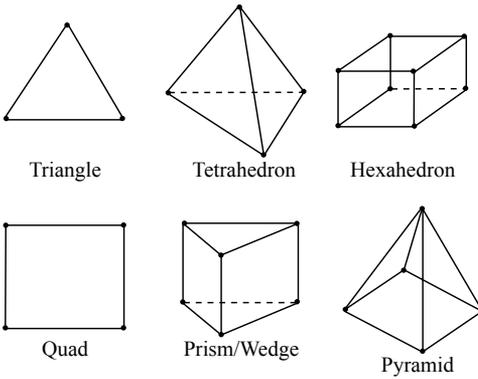
Figure 3
Element types that can be used in computational grids.

A series of line segments (2D) or planar faces (3D) connecting the boundaries of the domain are used to generate the elements. Structured grids are always quadrilateral (2D) or hexahedral (3D), and are such that every element has a unique address in I, J, K space, where I, J, and K are indices used to number the elements in each of the three computational directions (Figure 4).

4.1   4.2
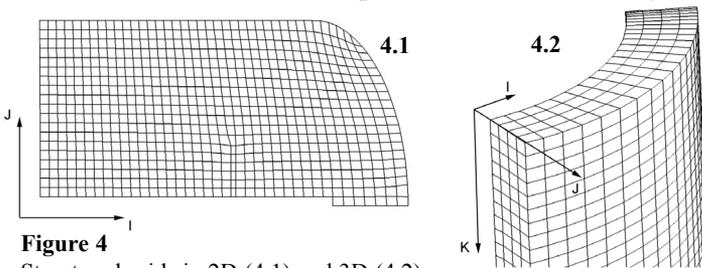
Figure 4
Structured grids in 2D (4.1) and 3D (4.2) showing the I, J, and K directions.

The I, J, and K directions can, but need not be aligned with the coordinate directions *x, y,* and *z*. Unstructured grids do not follow this addressing rule (Figure 5). Hybrid meshes are unstructured meshes that make use of different types of elements (triangles and quadrilaterals, for example). Block structured meshes use quadrilateral (2D) or hexahedral (3D) elements, and have I, J, K structures in multi-cell blocks rather than across the entire domain.

Figure 5
Unstructured grids using hexahedral elements (5.1) or a mixture of elements (5.2).
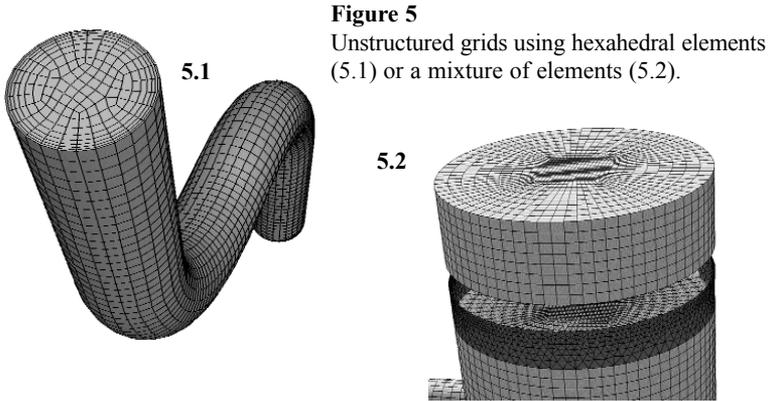
In general, the density of cells in a computational grid needs to be fine enough to capture the flow details, but not so fine that the overall number of cells in the domain is excessively large, since problems described by large numbers of cells require more time to solve. Nonuniform grids of any topology can be used to focus the grid density in regions where it is needed and allow for expansion in other regions.

In laminar flows, the grid near boundaries should be refined to allow the solution to capture the boundary layer flow detail. A boundary layer grid should contain quadrilateral elements in 2D and hexahedral or prism elements in 3D, and should have at least five layers of cells. For turbulent flows, it is customary to use a

wall function in the near-wall regions. This is due to the fact that the transport equation for the eddy dissipation has a singularity at the wall, where k (in the denominator in the source terms in Eq. (14)) is zero. Thus the equation for ε must be treated in an alternative manner. Wall functions rely on the fact that the flow in a turbulent boundary layer consists of a narrow viscous sub-layer and a broad, fully turbulent, or "log-law" layer in which the behavior is well documented. In particular, the shear stress due to the wall can be extracted from a linear relationship involving the log of the perpendicular distance to the wall. Guidelines exist so that the placement of the cell center in the cell nearest the wall lies outside the viscous sub-layer and inside the log-law layer. If these guidelines are followed, the wall shear stress will be captured correctly, resulting in the best possible predictions for pressure drop and heat transfer in the simulation.

3.2 Discretization of the Equations

Several methods have been employed over the years to solve the Navier-Stokes equations numerically, including the finite difference, finite element, spectral element, and finite volume methods. The focus of this chapter is on the finite volume method, which is described in detail below. Once the method and terminology have been presented, the other methods will be briefly discussed (Section 3.2.3).

To illustrate the discretization of a typical transport equation using the finite volume formulation (Patankar, 1980; Versteeg, 1995), a generalized scalar equation can be used with the rectangular control volume shown in Figure 6.1. The scalar equation has the form:

$$\frac{\partial(\rho\phi)}{\partial t} + \frac{\partial}{\partial x_i}(\rho U_i \phi) = \frac{\partial}{\partial x_i}\left(\Gamma \frac{\partial\phi}{\partial x_i}\right) + S' \tag{27}$$

The parameter Γ is used to represent the diffusion coefficient for the scalar ϕ. If ϕ is one of the components of velocity, for example, Γ would represent the viscosity. All sources are collected in the term S'. Again, if ϕ is one of the components of velocity, S' would be the sum of the pressure gradient, the gravitational force, and any other additional forces that are present. The control volume has a node, P, at its center where all problem variables are stored. The transport equation describes the flow of the scalar ϕ into and out of the cell through the cell faces. To keep track of the inflow and outflow, the four faces are labeled with lower case letters representing the east, west, north, and south borders. The neighboring cells also have nodes at their centers, and these are labeled with the capital letters E, W, N, and S. For the purpose of this example, flow in the 1D row of cells shown in Figure 6.2 is considered.

6.1
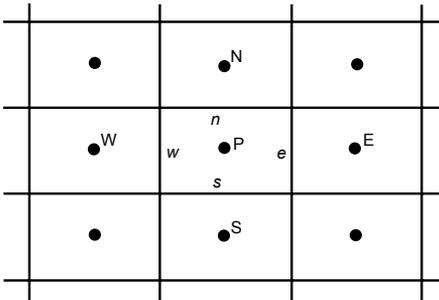
Figure 6
Simple 2D domain showing the cell centers and faces (6.1) and a 1D rectangular simplification of it (6.2).

6.2
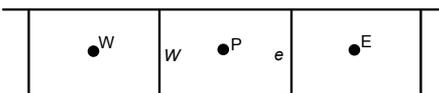
COMPUTATIONAL FLUID MIXING

The first step in the discretization of the transport equation is an integration over the control volume. The volume integral can be converted to a surface integral by applying the divergence theorem. Using a velocity in the positive x-direction, neglecting time-dependence, and assuming that the faces e and w have area A, the integrated transport equation takes the following form:

$$(\rho_e U_e \phi_e - \rho_w U_w \phi_w)A = \left(\Gamma_e \left[\frac{d\phi}{dx}\right]_e - \Gamma_w \left[\frac{d\phi}{dx}\right]_w \right)A + S \qquad (28)$$

where S is the volume integral of the source terms contained in S'. This expression contains four terms that are evaluated at the cell faces. To obtain the face values of these terms as a function of values that are stored at the cell centers, a discretization scheme is required.

3.2.1 Discretization Schemes

Since all of the problem variables are stored at the cell center, the face values (the derivatives, for example) need to be expressed in terms of cell center values. To do this, consider a steady-state conservation equation in one dimension without any source terms:

$$\frac{d}{dx}(\rho U \phi) = \frac{d}{dx}\left(\Gamma \frac{\partial \phi}{\partial x} \right) \qquad (29)$$

This equation can be solved exactly. On a linear domain that extends from $x = 0$ to $x = L$, corresponding to the locations of two adjacent cell nodes, with $\phi = \phi_0$ at $x = 0$ and $\phi = \phi_L$ at $x = L$, the solution for ϕ at any intermediate location (such as the face) has the form:

$$\phi = \phi_0 + (\phi_L - \phi_0) \frac{\exp\left(Pe \frac{x}{L} - 1 \right)}{\exp(Pe - 1)} \qquad (30)$$

The Peclet number, Pe, appearing in this equation is the ratio of the influence of convection to that of diffusion on the flow field.

$$\text{Pe} = \frac{\rho U L}{\Gamma} \tag{31}$$

Depending on the value of the Peclet number, different limiting behavior exists for the variation of ϕ between $x = 0$ and $x = L$. These limiting cases are discussed below, along with some more rigorous discretization, or differencing schemes that are in popular use today.

Central Differencing Scheme
For Pe = 0, there is no convection, and the solution is purely diffusive. This would correspond to heat transfer due to pure conduction, for example. In this case, the variable ϕ varies linearly from cell center to cell center, so the value at the cell face can be found from linear interpolation. When linear interpolation is used in general, i.e when both convection and diffusion are present, the discretization scheme is called central differencing. When used in this manner, as a general purpose discretization scheme, it can lead to errors and loss of accuracy in the solution. One way to reduce these errors is to use a refined grid, but the best way is to use another differencing scheme. There is one exception to this rule.   Central differencing is the preferred discretization scheme when the LES turbulence model is used.

Upwind Differencing Schemes
For Pe >>1, convection dominates, and the value at the cell face can be assumed to be identical to the upstream, or upwind value, i.e. $\phi_w = \phi_W$. When the value at the upwind node is used at the face, independent of the flow conditions, the process is called

first order upwind differencing. A modified version of first order upwind differencing makes use of multi-dimensional gradients in the upstream variable, based on the upwind neighbor and its neighbors. This scheme, which makes use of a Taylor series expansion to describe the upwind gradients, is called second order upwind differencing. It offers greater accuracy than the first order upwind method, but requires additional computational effort.

Power Law Differencing Scheme
For intermediate values of the Peclet number, $0 \leq Pe \leq 10$, the face value can be computed as a function of the local Peclet number, as shown in Eq. (30). This expression can be approximated by one that does not use exponentials, involving the Peclet number raised to an integral power. It is from this approximate form that the power law differencing scheme draws its name. This first order scheme is identical to the first order upwind differencing scheme in the limit of strong convection, but offers slightly improved accuracy for the range of Peclet numbers mentioned above.

QUICK Differencing Scheme
The QUICK differencing scheme (Leonard and Mokhtari, 1979) is similar to the second order upwind differencing scheme, with modifications that restrict its use to quadrilateral or hexahedral meshes. In addition to the value of the variable at the upwind cell center, the value from the next upwind neighbor is also used. Along with the value at the node P, a quadratic function is fitted to the variable at these three points and used to compute the face value. This scheme can offer improvements over the second order upwind differencing scheme for some flows with high swirl.

Choosing a Differencing Scheme

If the flow is aligned with the grid, first order differencing schemes such as upwind and power law differencing are acceptable. Flow in a straight pipe modeled with a hexahedral grid is one example where these schemes would be sufficient. However, since flow patterns in both static and stirred mixers do not, in general, satisfy this condition, especially if unstructured grids are used, second order differencing is recommended to reduce the numerical errors in the final solution. In general, first order schemes allow the error to reduce linearly with the grid spacing while second order schemes allow the error to reduce as the square of the grid spacing. A common practice in CFD is to obtain a partially converged solution using one of the first order schemes, and then switch to a higher order scheme to obtain the final converged result. The discretized schemes discussed above are summarized in Table 2.

Table 2: Summary of discretization schemes

Discretization Scheme	Description, Advantages, and Disadvantages
Central	Good when diffusion dominates. Assumes there is no convection, and that variables vary linearly from cell center to cell center. For convective flows, errors can be reduced by the use of a refined grid. This scheme is recommended for LES simulations.
First order upwind	Good when convection dominates and the flow is aligned with the grid. Assumes the face value for each variable is equal to the upstream cell center value. Stable, and a good way to start off a calculation. A switch to a higher order scheme is usually recommended once the solution has partially converged.
Second order upwind	Good for full range of Peclet numbers. Computes the face value for each variable from gradients involving the upwind neighbor and its neighbors.
Power law	Good for intermediate values of Peclet number. Computes the face value for each variable from gradients expressed in the form of a power law function. For high Peclet numbers, results are equivalent to first order upwind.
QUICK	Good for full range of Peclet numbers. Similar to second order upwind, but restricted to quadrilateral and hexahedral meshes.

3.2.2 Final Discretized Equation

Once the face values have been computed using one of the above differencing schemes, terms multiplying the unknown variable at each of the cell centers can be collected. Large coefficients multiply each of these terms. These coefficients contain information that includes the properties, local flow conditions, and results from previous iterations at each node. In terms of these coefficients, A_i, the discretized equation has the following form for the simple 2D grid shown in Figure 6:

$$A_P \phi_P = A_N \phi_N + A_S \phi_S + A_E \phi_E + A_W \phi_W = \sum_{i,neighbors} A_i \phi_i \tag{32}$$

For a complex, or even a simple flow simulation, there will be one equation of this form for each variable solved, in each cell in the domain. Furthermore, the equations are coupled, since, for example, the solution of the momentum equations will impact the transport of every other scalar quantity. It is the job of the solver to collectively solve all of these equations with the most accuracy in the least amount of time.

3.2.3 Alternative Numerical Techniques

As mentioned earlier, other methods for solving the Navier-Stokes equations exist. Two of these are described briefly below.

Finite Difference Method

The finite difference, or Taylor series formulation replaces the derivatives in Eq. (27) with finite differences evaluated at the variable storage sites (cell centers) using a truncated Taylor series expansion. The differences for each variable are computed using either the cell value or the adjacent neighbor values, depending on the order of the derivative. The variation of the variable

between storage sites is ignored during the solution process. While this is an acceptable method to solve for some simply varying functions, it is not the best choice for general purpose CFD analysis because the method is limited to simple grids, and does not conserve mass on coarse grids.

Finite Element Method
The finite element method uses piecewise linear or quadratic functions to describe the variation of the variable ϕ within a cell. By substituting the selected function into the conservation equation for each cell and applying the boundary conditions, a linear system of coupled equations is obtained. These equations are then solved (iteratively) for the unknown variable at all storage sites.

This method is popular for use with structural analysis codes and some CFD codes. In the early days of CFD, when structured orthogonal grids were used for most applications of the finite volume method, the finite element method offered the luxury of unstructured meshes with non-orthogonal elements of various shapes. Now that the use of unstructured meshes is common among finite volume solvers, the finite element method has been primarily used for certain focused CFD application areas. In particular, it is popular for flows that are neither compressible nor highly turbulent, and for laminar flows involving Newtonian and non-Newtonian fluids, especially those with elastic properties.

3.3 Solution Methods
The result of the discretization process is a finite set of coupled algebraic equations that need to be solved simultaneously in every cell in the solution domain. Because of the non-linearity of

the equations that govern the fluid flow and related processes, an iterative solution procedure is required. Two methods are commonly used. A segregated solution approach is one where one variable at a time is solved throughout the entire domain. Thus the *x*-component of the velocity is solved on the entire domain, then the *y*-component is solved, and so on. One iteration of the solution is complete only after each variable has been solved in this manner. A coupled solution approach, on the other hand, is one where all variables, or at a minimum, momentum and continuity, are solved simultaneously in a single cell before the solver moves to the next cell, where the process is repeated. The segregated solution approach is popular for incompressible flows with complex physics, typical of those found in mixing applications.

Typically, the solution of a single equation in the segregated solver is carried out on a subset of cells, using a Gauss-Seidel linear equation solver. In some cases, the solution time can be improved (i.e. reduced) through the use of an algebraic multigrid correction scheme. Independent of the method used, however, the equations must be solved over and over again until the collective error reduces to a value that is below a preset minimum value. At this point, the solution is considered converged, and the results are most meaningful. Converged solutions should demonstrate overall balances in all computed variables, including mass, momentum, heat, and species for example. Some of the terminology used to describe the important aspects of the solution process is defined below.

3.3.1 The SIMPLE Algorithm

For 3D simulations, the three equations of motion (Eq. (6)) and the equation of continuity (Eq. (5)) combine to form four equa-

tions for the four unknowns that are the pressure and the three velocity components. Because there is no explicit equation for the pressure, special techniques have been devised to extract it in an alternative manner. The most well known of these techniques is the SIMPLE algorithm, or Semi-Implicit Method for Pressure-Linked Equations (Patankar, 1980). Indeed, a family of algorithms has been derived from this basic one, each of which has a small modification that makes it well suited to one application or another.

The essence of the algorithm is as follows. A guessed pressure field is used in the solution of the momentum equations. (For all but the first iteration, the guessed pressure field is simply the last updated one.) The new velocities are computed, but these will not, in general, satisfy the continuity equation, so corrections to the velocities are determined. Based on the velocity corrections, a pressure correction is computed which, when added to the original guessed pressure, results in an updated pressure. Following the solution of the remaining problem variables, the iteration is complete and the entire process repeated.

3.3.2 Residuals

If the algebraic form of a conservation equation in any control volume (Eq. (32)) could be solved exactly, it would be written as:

$$A_P \Phi_P - \sum_{i,neighbors} A_i \Phi_i = 0 \qquad (33)$$

Since the solution of each equation at any step in an iterative calculation is based on inexact information, originating from initial guessed values and refined through repeated iterations, the right hand side of the above equation is always non-zero. This non-

zero value represents the error, or residual in the solution of the equation in the control volume.

$$A_P \Phi_P - \sum_{i,neighbors} A_i \Phi_i = R_P \tag{34}$$

The total residual is the sum over all cells in the computational domain of the residuals in each cell.

$$\sum_{P,cells} R_P = R \tag{35}$$

Since the total residual, R, defined in this manner, is dependent upon the magnitude of the variable being solved, it is customary to either normalize or scale the total residual to gauge its changing value during the solution process. While normalization and scaling can be done in a number of ways, it is the change in the normalized or scaled residuals that is important in evaluating the rate and level of convergence of the solution.

3.3.3 Convergence Criteria

The convergence criteria are preset conditions for the (usually normalized or scaled) residuals that determine when an iterative solution is converged. One convergence criterion might be that the total normalized residual for the pressure equation drop below 1×10^{-3}. Another might be that the total scaled residual for a species equation drop below 1×10^{-6}. Alternatively, it could be that the sum of all normalized residuals drop below 1×10^{-4}. For any set of convergence criteria, the assumption is that the solution is no longer changing when the condition is reached, and that there is an overall mass balance throughout the domain. When additional scalars are being solved (heat and species, for example), there should be overall balances in these scalars as well.

44

Whereas the convergence criteria indicate that overall balances probably exist, it is the wise engineer who will examine reports to verify that indeed they do.

3.3.4 Underrelaxation

The solution of a single differential equation, solved iteratively, makes use of information from the previous iteration. If ϕ_n is the value of the variable from the previous iteration and ϕ_{n+1} is the new value, then some small difference or change in the variable brings the variable from the old value to the new one.

$$\phi_{n+1} = \phi_n + \Delta\phi \qquad\qquad (36)$$

Rather than use the full computed change in the variable, $\Delta\phi$, it is often necessary to use a fraction of the computed change when several coupled equations are involved.

$$\phi_{n+1} = \phi_n + f\Delta\phi \qquad\qquad (37)$$

This process is called underrelaxation, and underrelaxation factors, f, typically range from 0.1 to 1.0, depending on the complexity of the flow physics (laminar flow or turbulent reacting flow, for example), the variable being solved (pressure or momentum), the solution method being used, and the state of the solution (during the first few iterations or near convergence). Underrelaxation makes the convergence process stable, but slower. Guidelines exist for the optimum choices for underrelaxation factors for a variety of conditions. As the solution converges, the underrelaxation factors should be gradually raised to ensure convergence that is both rapid and stable at all times.

3.3.5 Numerical Diffusion

Numerical diffusion is a source of error that is always present in CFD, owing to the fact that approximations are made during the process of discretization of the equations. It is so named because it presents itself as equivalent to an increase in the diffusion coefficient. Thus in the solution of the momentum equation, the fluid will appear more viscous; in the solution of the energy equation, the solution will appear to have a higher conductivity; in the solution of the species equation, it will appear that the species diffusion coefficient is larger than in actual fact. These errors are most noticeable when diffusion is small in the actual problem definition.

To minimize numerical diffusion, two steps can be taken. First, a higher order discretization scheme can be used, such as the QUICK or second order upwinding schemes discussed earlier. Second, the grid can be built so as to minimize the effect. In general, numerical diffusion is more of a problem on coarse grids, so it is wise to plan ahead and avoid coarse meshes in regions where the most accuracy is sought. Numerical diffusion is usually less of a problem with quadrilateral or hexahedral meshes, provided the flow is aligned with the mesh. Unfortunately, the flow is rarely aligned with the mesh throughout the entire flow field, so some degree of numerical diffusion is unavoidable.

3.3.6 Time-Dependent Solutions

To solve a time-dependent problem, the time derivative appearing in Eq. (27) must be discretized. If $F(\phi)$ is the spatially discretized part of Eq. (27), the time derivative can be approximated to first order as:

$$\frac{\phi^{n+1} - \phi^{n}}{\Delta t} = F(\phi) \qquad (38)$$

In this expression, ϕ^n is the solution at time t, and ϕ^{n+1} is the solution at time $t+\Delta t$. While certain flow conditions, such as compressible flow, are best suited to an explicit method for the solution of Eq. (38), an implicit method is usually the most robust and stable choice for a wide variety of applications, including mixing. The major difference between the explicit and implicit methods is whether the right hand side of Eq. (38) is evaluated at the current time $(F(\phi) = F(\phi^n))$ or at the new time $(F(\phi) = F(\phi^{n+1}))$. The implicit method uses the latter:

$$\phi^{n+1} = \phi^n + \Delta t F\left(\phi^{n+1}\right) \tag{39}$$

The assumption at the core of this quasi-steady approach is that the new value of the variable ϕ prevails throughout the entire time step, which takes the solution from time t to time $t+\Delta t$.

3.4 Parallel Processing

Parallel processing is a procedure in which a large calculation can be performed on two or more processors working in parallel. The processors can reside on the same (multiprocessor) computer, or can be on a network of computers. For the calculation to run on the processors in a parallel fashion, the calculation domain (the computational grid) must be divided into partitions, or sub-domains. The equations in each partition are solved simultaneously on the multiple processors (using the segregated or coupled approach), and the results at the boundaries of the partitions are communicated to the neighbor partitions on a regular basis. As the number of nodes increases, the computation time for each node decreases, and the communication between partitions increases. In this limit, the efficiency of parallel computing decreases. Recent advances in parallel algorithms have pushed back this limiting behavior, however.

COMPUTATIONAL FLUID MIXING

IV

STIRRED TANK MODELING USING EXPERIMENTAL DATA

Stirred tanks typically contain one or more impellers mounted on a shaft, and optionally, baffles and other internals. While it is a straightforward matter to build a 3D mesh to contour to the space between these elements, the mesh must be built so that the solution of the flow field incorporates the motion of the impeller. This can be done in two ways. First, the impeller geometry can be modeled directly, or explicitly, and the grid and solution method chosen so as to incorporate the motion of the impeller using either a steady-state or time-dependent technique. This approach is discussed in detail in Chapter V. Second, the motion of the impeller can be modeled implicitly, using time-averaged experimental velocity data to represent the impeller motion. The second approach is the subject of this section, which is divided into the following parts:

Section 4.1: Impeller modeling with velocity data
Section 4.2: Using experimental data
Section 4.3: Treatment of baffles in 2D simulations
Section 4.4: Combining the velocity data model with other physical
            models

49

COMPUTATIONAL FLUID MIXING

4.1 Impeller Modeling with Velocity Data

When modeling the impeller using velocity data, the time-aver-
aged velocities in the outflow of the impeller are prescribed, and
the CFD solver calculates the flow in the remainder of the vessel.
An illustration of this process is shown in Figure 7 for a radial
flow impeller. The parabolic velocity profile in the impeller out-
flow region is prescribed as a boundary condition in the simula-
tion, and the well-known radial flow pattern with circulation
loops above and below the impeller results from the CFD calcu-
lation. It is important to note that the volume swept by the
impeller is also part of the model but that, other than for the fixed
velocities in the outflow region, it is treated as part of the fluid
domain by the CFD solver. Figure 7 also illustrates the fact that
for this particular case it is indeed sufficient to prescribe the
velocities in the impeller outflow only in order to obtain a good
flow field prediction. Bakker and Van den Akker (1994) pre-
sented a quantitative validation for this case.
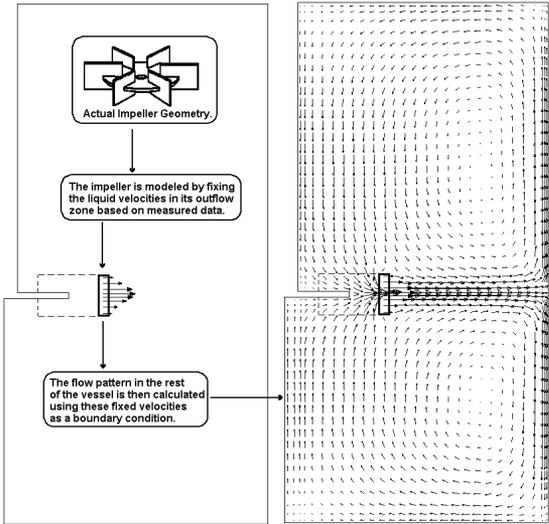
Figure 7
Velocity data measured radially outside a radial flow impeller is applied to a 2D CFD simulation, resulting in the well known double loop flow pattern.

Over the years, practical experience has demonstrated that it is usually sufficient to prescribe the velocity data only along the edges of the impeller where the flow exits. One or two edges of the impeller are typically needed for this purpose. For an impeller that creates a purely radial flow pattern, such as the radial flow impeller of Figure 7, prescribing the velocities on the side of the impeller is sufficient, since flow is drawn into the impeller at the top and bottom edges.

In general for all impeller types, all three velocity components should be prescribed in the discharge region. For turbulent flow it is also recommended that values for the turbulent kinetic energy, k and dissipation rate, ε be prescribed. The turbulent kinetic energy can be computed from measured fluctuations in the velocity components, using Eq. (12). Using k, the eddy dissipation can be calculated using

$$\varepsilon = \frac{k^{3/2}}{L_t} \tag{40}$$

where L_t is a characteristic turbulent length scale in the outflow of the impeller. One commonly used relationship is $L_t = W_b/4$, where W_b is the width of the impeller blade.

Figure 8 shows where to prescribe the velocity data for various cases, including the previously discussed radial flow impeller (Figure 8.1). For a down-pumping impeller that creates a purely axial flow pattern (Figure 8.2), liquid will enter the impeller from the top and the side, and exit the impeller on the bottom. In such a case it is sufficient to prescribe the liquid velocities along the bottom edge only. For an up-pumping impeller under the same conditions, the velocities would be prescribed along the top edge.

COMPUTATIONAL FLUID MIXING

When an axial flow impeller operates in the laminar flow regime, however, it will have a combined axial-radial flow (Figure 8.3). On the bottom of the impeller, flow both enters and exits depending on the radial location. Furthermore, flow exits the impeller on the side. On the top of the impeller, flow enters but does not exit. Therefore, for this situation the proper modeling method is to prescribe complete velocity profiles on both the bottom and the side edges. While it is not in general recommended to prescribe all velocity components on the top of the impeller as well, for laminar flow conditions the prediction of the swirling flow pattern in the top of the vessel can be improved by prescribing the tangential velocity component only along this edge, in addition to the prescriptions along the side and bottom. For an up-pumping impeller, the velocities should be prescribed along the top and the side edges, with the swirl (optionally) prescribed along the lower edge for laminar flows only.

One exception to the rule that velocities should be prescribed in the impeller discharge region occurs when a down-pumping axial flow impeller is mounted very close to the vessel bottom (or an up-pumping impeller close to the liquid surface). Such cases present several difficulties. On the experimental side, measuring velocities in regions close to walls can be difficult and may result in inaccuracies. In the CFD simulation, there may be only a few computational cells between the vessel bottom and the impeller. In these circumstances, good results can often still be obtained if the velocities are prescribed at the top inflow of the impeller (Figure 8.4).

8.1
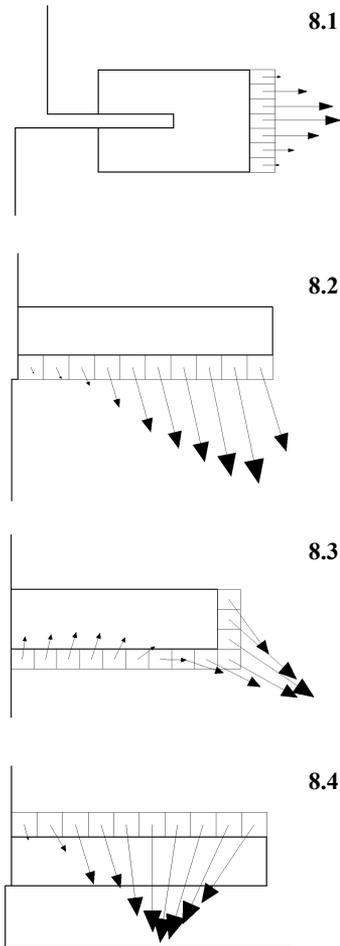
Figure 8
This figure shows where to prescribe impeller boundary conditions for:

8.1) a radial flow impeller in the turbulent flow regime,

8.2) an axial flow impeller in the turbulent flow regime,

8.3) an axial flow impeller operating in the laminar flow regime,

8.4) an axial flow impeller close to the vessel bottom.

8.2

8.3

8.4

4.2 Using Experimental Data

Several experimental methods are available for measuring the velocities imparted to the fluid by a working impeller. These include laser Doppler velocimetry, or LDV, and particle image velocimetry, or PIV. Under ideal circumstances, the velocity data

prescribed for a simulation would have been obtained from measurements made on an identical system. In practice, however, this is rarely the case. The experimental data that is available was most likely obtained for conditions that are different from the system being modeled. Nonetheless, several scaling rules can be applied to the existing data so that appropriate velocity profiles for the case at hand can be generated.

The first step involves the normalization of the available data. Typically the measured liquid velocities are normalized by the impeller tip speed, U_{tip}, used during the experiment. The turbulent kinetic energy is usually normalized by U_{tip}^2. The eddy dissipation can be normalized by U_{tip}^3/D, with a possible constant of proportionality. Radial measurement locations are typically normalized by the impeller radius, R, and axial locations by the impeller blade height, z, measured from the impeller centerline.

To perform the simulation, profiles for the liquid velocities, k, and ε are obtained by multiplying the normalized profiles by the actual U_{tip}, U_{tip}^2, and U_{tip}^3/D, respectively. The locations at which the velocity data are available are calculated by multiplying the normalized measurement locations by the actual impeller radius or blade height.

When prescribing the velocity data above or below the impellers, it is recommended that the computational grid be constructed such that the center of the cells where the velocities are prescribed, fall within a quarter cell height of the normalized axial measurement locations. Similarly when prescribing data at the side of the impeller, it is recommended that the cell centers are within a quarter cell width of the normalized radial measurement

locations. For both cases, interpolation can then be used to determine the velocity values at the radial and axial grid locations of the individual cell centers, respectively.

The exact shape of the velocity profile in the outflow of an impeller is not solely dependent upon the impeller itself. Rather, it is affected by such variables as the impeller Reynolds number, impeller off-bottom distance C/T, and impeller diameter D/T. If the flow is fully turbulent (i.e. Re > 10⁴), the impeller outflow profiles are typically independent of Reynolds number. If the flow is transitional or laminar, however, care should be taken so that the velocity profiles used were either measured at a similar Reynolds number, or that the prescribed velocities are being interpolated from datasets measured over a range of Reynolds numbers. Similarly, for impeller off-bottom clearance and diameter, if data for various C/T and D/T values are available, interpolations can be used to obtain the prescribed velocities for the actual conditions.

4.3 Treatment of Baffles in 2D Simulations

As mentioned earlier, the time-averaging method used to record velocity data for an impeller makes the data useful for 2D simulations in the radial-axial plane, where angular- (and therefore time-) dependence of the geometry and flow field is ignored. While ignoring the angular dependence of the impeller motion can be done in this manner, the angular dependence of the baffles needs to be addressed as well. Baffles are used to reduce the swirl introduced by the rotating impeller. One way of including this effect in a 2D simulation is to omit the swirling component of the velocity data in the numerical simulation, using only the radial and axial components instead. Another way to model baf-

fles is to set a boundary condition of zero swirl in the baffle region in the 2D simulation. By setting the boundary condition on the swirl only, the axial and radial velocities can be computed in the baffle region as they are in the remainder of the vessel.

4.4 Combining the Velocity Data Model with Other Physical Models

The steady-state, implicit impeller model, which uses time-averaged experimental data, can be used to model other steady-state and time-dependent processes, as described below. Because of its simplicity, it has no effect on other scalar transport in the domain. The models that do require special consideration are those involving multiple phases, with separate sets of momentum boundary conditions, as described below. Species blending is also discussed, because it is a calculation that is commonly performed in conjunction with the implicit impeller model.

4.4.1 VOF Model

In stirred tank applications, the VOF model is useful for tracking the shape of the liquid surface during operation. This includes the transition to a parabolic shape during startup, which can lead to the (undesired) drawdown of air. The velocity data model can be used in 2D or 3D for simulations of this type. The VOF model can have a steady or time-dependent implementation, and both are fully compatible with this steady-state treatment of the impellers.

If air drawdown does occur, caution is needed. If air passes through cells where large momentum sources exist, resulting from the velocity data boundary conditions, the liquid/air interface will be broken, resulting in many small bubbles that will mix

with the liquid. The VOF model is not equipped to handle this condition accurately, so the simulation should be terminated at this point. Thus while the model can be used to predict if draw-down will occur, it should not be used to predict the flow conditions afterwards.

4.4.2 Multiphase

Both solids suspension and gas sparging can be simulated using an experimental data model for the impeller. The manner in which the multiphase parameters are input depends upon the multiphase model being used. For solids suspension, an Eulerian granular multiphase model is recommended, and separate sets of momentum equations are used for the liquid and solids phases. This model, run in a time-dependent fashion, is fully compatible with the time-averaged representation of the impellers. Experimental velocity data is set as a boundary condition independently for each of the phases. Note, however, that there is usually some degree of slip between the fluid and granular phases. Thus the velocities used to represent the impeller for a pure liquid need to be adjusted somewhat for the granular phase. This can be accomplished by estimating the slip velocity between the two phases. The measured data can be used to represent the impeller for the fluid phase, and a corrected set of data, obtained by subtracting the slip velocity from the experimental data, can be used to represent the impeller for the solids phase.

Gas sparging can be modeled using the Eulerian multiphase model or the algebraic slip mixture model. For the Eulerian multiphase model, two sets of momentum equations are used, and the same comments regarding the slip velocity between phases apply, although the issue is not as critical. That is, the velocity data used

for the gas phase could be corrected slightly from the liquid phase velocities, but need not be because the gas phase has so little inertia compared to the liquid phase. When the algebraic slip mixture model is used, separate boundary conditions are not required for the individual phases, so a correction of the velocity data is not required.

Another consideration in the case of gas-liquid mixtures is the impact of the impeller on the gas bubble size. In an actual stirred tank, the momentum of the rotating impeller often acts to break up gas bubbles as they pass through the region. This reduces the bubble size and can lead to an increase in the gas holdup, as well as a change in the momentum exchange term (drag) between the phases. When experimental data is used, this phenomenon is missing from the formulation, but can often be incorporated into the calculation if subroutines, written by the user, are available to modify the model in the commercial software.

4.4.3 Turbulence
The use of a transient turbulence model, such as the large eddy simulation model, is inconsistent with the experimental data formulation because the latter is intrinsically steady-state. All of the RANS models, however, are fully compatible with the velocity data approach.

4.4.4 Species Blending
When a neutrally buoyant tracer, one with the same fluid properties, is added to the liquid in a vessel, a simplified approach to predicting the mixing time can be used. Rather than model the complete set of transport equations in a transient manner, the steady-state flow field can be computed first, including the

inflow and outflow for the anticipated tracer and resulting mixture, respectively. Prior to beginning the transient species calculation for the tracer, the calculation of the flow field variables (pressure, momentum, and turbulence) can be disabled, since the overall properties of the mixture will not change. Thus the dispersion of the tracer species can be tracked by solving only a single scalar transport equation. (The same technique can be used for heat transfer if the properties are the same and not temperature-dependent.) This method for computing species blending is fully compatible with the experimental data representation of the impellers.

COMPUTATIONAL FLUID MIXING

V

STIRRED TANK MODELING USING THE ACTUAL IMPELLER GEOMETRY

To model the geometry of the impeller exactly, a 3D simulation must be performed. A number of solution approaches are available to incorporate the motion of the impeller, and the computational grid used must be able to adapt to the solver method employed. The models in popular use today are reviewed in the following sections:

Section 5.1:   Rotating frame model
Section 5.2:   Multiple reference frames model
Section 5.3:   Sliding mesh model
Section 5.4:   Snapshot model
Section 5.5:   Combining the geometric models with other
               physical models

Particular attention is paid to the sliding mesh model, the most rigorous of them all. The solver methods described are all designed to capture the motion of a rotating impeller in a station-

ary tank, but they vary in accuracy. Three of the models are steady-state and one is time-dependent.

5.1 Rotating Frame Model

The rotating frame model solves the momentum equations for the entire domain in a rotating frame. The Coriolis force is included in the process. Problems solved in a rotating frame typically use the angular velocity of the primary rotating component, Ω, as the angular velocity of the frame. In stirred tanks, the impeller serves this purpose, so the frame is assumed to rotate with the impeller. Thus the impeller is at rest in the rotating frame. The tank, however, rotates in the opposite direction, so must have a rotational boundary condition of $-\Omega$. If baffles exist, they would need to rotate into the fluid with the same angular velocity, $-\Omega$. Unfortunately, this simple steady-state model is not equipped to handle the motion of elements such as baffles into or through the fluid. The approach is therefore only useful for unbaffled tanks with smooth tank walls that are geometrically equivalent to a perfect surface of revolution. Thus an unbaffled cylindrical tank with an axisymmetric bottom shape and no angular-dependent internals could be simulated in this manner. Vessels with baffles, dip tubes, or inflow/outflow ports could not.

5.2 Multiple Reference Frames Model

A modification of the rotating frame model is the multiple reference frames, or MRF model (Luo *et al.*, 1994). The modification is that more than one rotating (or non-rotating) reference frames can be used in a simulation. This steady-state approach allows for the modeling of baffled stirred tanks and tanks with other complex (rotating or stationary) internals. A rotating frame is used for the region containing the rotating components while a

stationary frame is used for regions that are stationary (Figure 9). In the rotating frame containing an impeller, the impeller is at rest. In the stationary frame containing the tank walls and baffles, the walls and baffles are at rest. The fact that multiple reference frames can be used means that multiple impeller shafts in a rectangular tank can each be modeled with separate rotating frames (with separate rotation frequencies) while the remaining space can be modeled with a stationary frame.
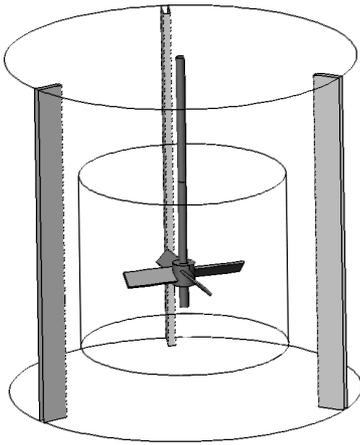
Figure 9
Cylindrical mixing tank with an MRF boundary surrounding the impeller.

The grid used for an MRF solution must have a perfect surface of revolution surrounding each rotating frame. The momentum equations inside the rotating frame are solved in the frame of the enclosed impeller while those outside the rotating frame are solved in the stationary frame. A steady transfer of information is made at the MRF interface as the solution progresses. While the solution of the flow field in the rotating frame in the region surrounding the impeller imparts the impeller rotation to the region outside this frame, the impeller itself does not move during this type of calculation. Its position is static. If the impeller is mounted on a central shaft in a baffled tank, this means that the

orientation of the impeller blades relative to the baffles does not change during the solution. If the interaction between the impeller and baffles is weak, the relative orientation of the impeller and baffles does not matter. If the interaction is strong, however, the solution with the impeller in one position relative to the baffles will be different from that with the impeller in a different position. The model is therefore recommended for simulations in which the impeller-baffle interaction is weak. Note however, that if the solution is to be used to obtain spatially averaged, macroscopic properties of the flow field, such as power draw, the orientation of the impeller relative to the baffle may not matter. The careful engineer will perform two solutions with the impeller in two different locations and use both results (averaging them, for example) rather than just one.

A modified version of the MRF model is the mixing plane model, in which the variables at the MRF boundary are spatially averaged in the circumferential direction prior to being passed from one side to the other. After the averaging process, all angular dependence on the boundary is eliminated, so the variables are functions of radial and axial position only. This approach is popular for turbomachinery, where many closely spaced rotors and stators are in relative motion. It has not had widespread use in the mixing community, however, owing in part to asymmetries in the flow field that are common in stirred tanks. For example, a tracer species introduced through a single dip tube on the side of the vessel would appear to be uniformly distributed on the interface shortly after reaching it, which is clearly unphysical. As another example, any stirred tank with inflow and outflow ports could have flow through the MRF interface that is not unidirectional. When the averaging process is done, this condition could

also result in unphysical results. The mixing plane approach is therefore not recommended for most stirred tank applications.

5.2.1 Validation of the MRF Model

To validate the MRF model, a Lightnin A310, operating in a baffled vessel ($Re = 4.6 \times 10^5$), was simulated using a number of turbulence models (Marshall, *et al.*, 1999). Results for the velocity field, power number and flow number were compared to measurements performed by Weetman (1997). The vessel used for the simulation had a diameter $T = 1.22m$ (Figure 10.1). The A310 impeller (with surface grid shown in Figure 10.2) had a diameter and off-bottom clearance of $D/T = C/T = 0.352$. A 120° sector of the domain was modeled using a grid of approximately 150,000 hexahedral cells.
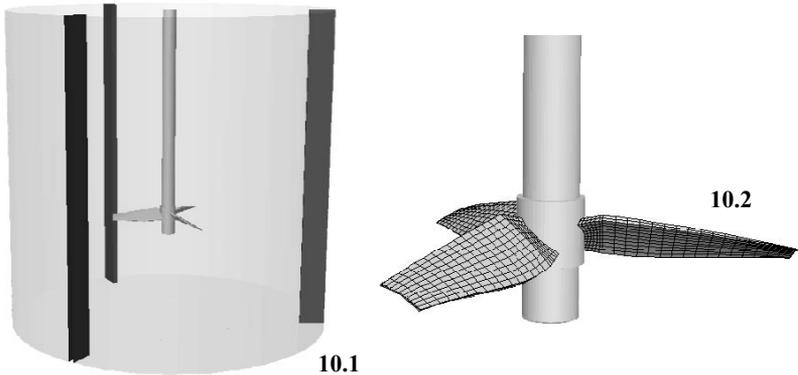
Figure 10
Tank containing an A310 impeller (10.1) and grid detail for the impeller surface (10.2).

Figure 11 shows a comparison of the velocity data from the LDV measurements with the velocities in a non-baffle plane computed by the MRF model, using RSM for turbulence. The CFD calculation picks up the features of the flow field correctly. In Table

65

3, the results for flow number, N_Q (Section 6.4.2), and power number, N_P (Section 6.4.1), show good agreement for all turbulence models. The power drawn by the impeller was computed by integrating the pressure on the impeller blades to obtain the torque. The flow rate was computed by integrating the flow through a circular discharge area below the impeller.

11.1

11.2
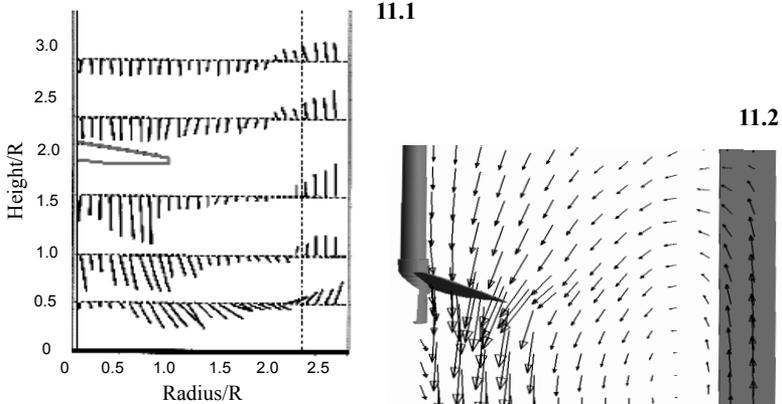
Figure 11
Experimental data from Weetman (1997) (11.1) and the CFD solution using the MRF model for the impeller and RSM for turbulence (11.2).

Turbulence Model	N_Q	N_P
Experiment*	0.56	0.30
Standard k-ε	0.50	0.30
RNG k-ε	0.53	0.28
Realizable k-ε	0.52	0.29
RSM	0.51	0.29

Table 2
Results of the MRF impeller model with several turbulence models as compared to experiment (*Experimental data provided by the impeller manufacturer).

5.3 Sliding Mesh Model

The sliding mesh model is a time-dependent solution approach in which the grid surrounding the rotating component(s) physically moves during the solution (Figure 12). The velocity of the impeller and shaft in the moving mesh region is zero, as is the velocity of the tank, baffles, and other internals in the stationary mesh region. The motion of the impeller is realistically modeled because the grid surrounding it moves as well, giving rise to a time-accurate simulation of the impeller-baffle interaction. The motion of the grid is not continuous. Rather, it is in small, discrete steps. After each such motion, the set of conservation equations is solved in an iterative process until convergence is reached. The grid moves again, and convergence is once again obtained from an iterative calculation. During each of these quasi-steady calculations, information is passed through the interface from the rotating to the stationary regions and back again.

In order to rotate one mesh relative to another, the boundary between the meshes needs to be a surface of revolution. When in its initial (unrotated) position, the grid on this boundary must
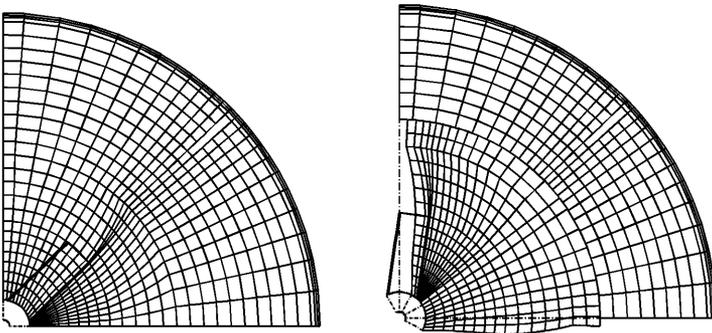
Figure 12
Sliding mesh in two orientations (shown in 2D).

have two super-imposed surfaces. During the solution, one will remain with the rotating mesh region, and the other will remain with the stationary mesh region. At any time during the rotation, the cells will not (necessarily) line up exactly, or conform to each other. When information is passed between the rotating and stationary grid regions, interpolation is required to match each cell with its many neighbors across the interface.

The sliding mesh model is the most rigorous and informative solution method for stirred tank simulations. Transient simulations using this model can capture low frequency (well below the blade passing frequency) oscillations in the flow field (Bakker *et. al.,* 2000 and Roussinova *et al.,* 2000) in addition to those that result from the periodic impeller-baffle interaction.

5.3.1 Solution Procedures

Because this is a transient model involving the motion of the impeller, starting the simulation with the impeller at rest is analogous to modeling start-up conditions. After a period of time the flow field reaches periodic steady-state, but this period of time may correspond to dozens of revolutions. If the goal of the simulation is to study the periodic steady state conditions, minimizing the time spent reaching this state is desirable.

One way to rapidly pass through the start-up conditions is to move the impeller by large increments each time step in the early stage of the calculation. If the model is a 90° sector, for example, the first few revolutions of the impeller can be modeled using a coarse time step that corresponds to a 30° displacement. The time step can then be refined to correspond to a 10° displacement, and refined again (and again) until the desired temporal and spatial

accuracy is achieved. The solutions during these initial coarse time steps do not need to be perfectly converged, provided the simulation involves a single fluid phase and there are no inflow and outflow boundaries. In these instances, improved convergence can be obtained in the later stages of the calculation.

An alternative way to by-pass the calculation of the start-up period is to solve for a steady-state solution first using the MRF model. The MRF model (Section 5.2) provides a solution for the moving impeller at a fixed orientation relative to the baffles. Tools are available in commercial codes to use the solution data from the MRF simulation and apply it to the sliding mesh simulation as an initial condition. A moderately coarse time step can be used initially (say, corresponding to a 10° rotation, as in the above example) and reduced at a quicker rate than would otherwise be advisable. This approach can also be used if there are inflow and outflow boundaries present or if a multiphase calculation is to be performed. In the case of multiphase flows, however, care must be taken to wait until the periodic steady-state condition has been reached before introducing the secondary phase.

5.3.2 Validation of the Sliding Mesh Model

One validation of the sliding mesh model was presented in a paper by Bakker, *et al.* (1997). A pitched blade turbine was operated in a baffled vessel with diameter T = 0.3m under laminar conditions (Re = 40). The impeller diameter and off-bottom clearance were such that D/T = C/T = 1/3. A 90° sector of the stirred tank was modeled using approximately 50,000 cells.

Figure 13 shows a comparison between LDV data on the left and CFD results on a mid-baffle plane on the right. Because the

impeller was operating at a low rotational speed, its discharge was more radial than axial. This structure is captured by the CFD model, in agreement with the experimental data, where circulation loops above and below the impeller can be seen. Turbulent calculations for this system operating at higher Reynolds numbers were also performed. Results for the flow number (Section 6.4.2), computed throughout both laminar and turbulent regimes, are in excellent agreement with values based on LDV measurements, as shown in Figure 14.
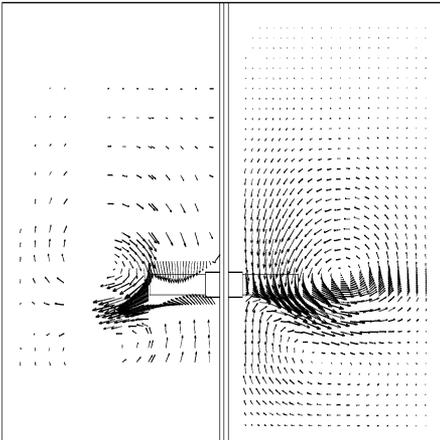
Figure 13
Comparison of LDV data (left) and sliding mesh CFD results (right).
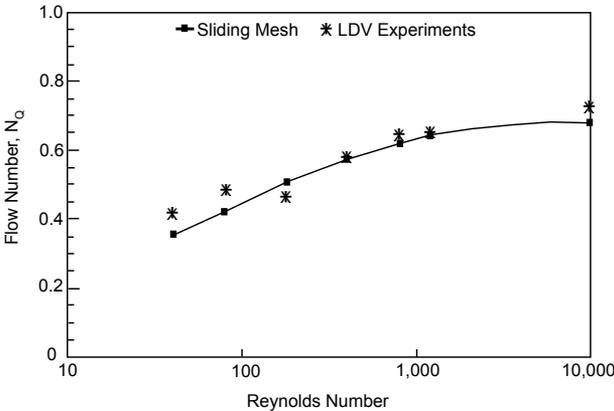
Figure 14
Flow number based on experimental measurements and computed by the sliding mesh model.

5.3.3 Unstable Flows

In recent years, much attention has been paid to instabilities that are observed in stirred tanks. These instabilities typically have frequencies that are low compared to the impeller frequency, and involve the slow asymmetric wobble of material or momentum from one side of the vessel to the other. Instabilities of this type can be predicted using the sliding mesh technique on a 360° model of a stirred tank, particularly if the LES turbulence model is used (Bakker *et al.,* 2000 and 2001).

5.4 Snapshot Model

The snapshot model (Ranade, 1996) is a steady-state approach that captures the flow field at a single instant in time, when the impeller position relative to the baffles is fixed. When the impeller is rotating, the leading face of the blade exerts a force on the fluid in front of it, and acts to push the fluid away. Behind the rotating blade, there is a void of low pressure, which acts to pull the surrounding fluid in. These two complementary functions can be represented as balanced mass sources in front of and in back of the impeller blade, and this premise is the basis of the snapshot model. A grid is built with the impeller in one position relative to the baffles, and a steady-state solution is performed. Mass sources in front of and behind the impeller blade are used to simulate the action of the impeller as if it were rotating. The flow field is therefore characteristic of a fully developed flow for a rotating impeller, but is limited to a snapshot of the motion when the impeller is in the single position described by the model.

5.5 Combining the Geometric Impeller Models with Other Physical Models

The geometric impeller models described above can be used to

model both steady-state and time-dependent processes, but attention must be paid to the time-scales, where appropriate, and other special requirements of each. In this section, some of these considerations are reviewed for the two most popular of the geometric formulations: the MRF and sliding mesh models.

5.5.1 VOF Model

In stirred tank applications, the VOF model is useful for tracking the shape of the liquid surface during operation. Even though the steady-state shape of the surface is usually of interest, a transient VOF formulation is usually the best way to obtain it. With this in mind, either the steady-state MRF or transient sliding mesh model can be used for this purpose. If the MRF model is used, the gradual change in the free surface can be predicted using the VOF method. Note, however, that because the orientation of the impeller relative to the baffles is fixed, any irregularities in the free surface that result from the impeller rotation will not be captured. If these details are important, the sliding mesh model should be used.

When the VOF model is solved in conjunction with the sliding mesh model, the smallest required time step for the two models must be used. Since a smaller time step is often required for the VOF calculation than for the sliding mesh calculation, this means that the motion of the impeller will advance in time at a slower rate than is necessary for a calculation involving the sliding mesh model alone. One way to circumvent this problem is to use the sliding mesh model to obtain periodic steady state conditions using a single fluid first, and then introduce the second fluid with the VOF model and continue the transient calculation until a new periodic steady state is reached. For simple cases in which the

free surface is axisymmetric, an implicit impeller model using fixed velocity data (Chapter IV) may be preferable for use with the VOF calculation.

5.5.2 Multiphase

Gas-liquid or liquid-solids mixtures can be solved using the Eulerian multiphase or ASM model in conjunction with either the sliding mesh or MRF model. Whereas the common goal of free surface modeling using VOF is to obtain the steady-state shape of the liquid interface, the goal of multiphase modeling can be to examine the unsteady behavior of the mixture as well as to predict the final settling of solids or final gas holdup. The advantage of using the MRF model is that its steady-state basis can be combined with the time-stepping needed for complex multiphase flows. The disadvantage, however, is that the fixed orientation of the impeller blade with the baffles introduces error in the transient behavior by ignoring the impact of the impeller-baffle interaction on the flow.

For cases in which the transient behavior of the process is of interest, the sliding mesh model should be used instead. Here, the same issues apply that are important for VOF modeling. Generally speaking, a smaller time step is required for the Eulerian multiphase model than for the sliding mesh calculation. It is good practice to obtain a periodic steady state solution of the single phase liquid first using the sliding mesh model prior to introducing the additional phases. The development of the solids suspension or gas holdup can then be computed most accurately in the presence of the rotating impeller.

5.5.3 Turbulence

As was discussed in Chapter II, there are several steady-state turbulence models in widespread use today. These so-called RANS models address a time-averaged state of the fluid such that all turbulent fluctuations are represented by averaged values.   The RANS models are often used with both the MRF and sliding mesh models, as well as with many other transient models used in CFD analysis. This practice is justified in part because the time scales of turbulence fluctuations are assumed small compared to those of the other processes being modeled, such as the blade passing time in a stirred tank.   It has also been justified because until recently, other more rigorous treatments have not been available in commercial software or solvable in a realistic time on the computers of the day.

The large eddy simulation, or LES model (Section 2.1.3), is a fairly recent model to appear in commercial software. It offers considerably more rigor than the RANS models. It makes use of a steady-state model for the smallest turbulent eddies, but treats the large scale eddies in a transient manner. The use of LES is inconsistent with the use of the MRF modeling approach, because the approximation introduced with the MRF model is on a longer time scale than the detail offered by the LES calculation. The use of LES with the sliding mesh model, on the other hand, is a powerful combination that has demonstrated great potential for capturing not just small scale fluctuations, but large scale fluctuations as well, including instabilities with frequencies that are several times larger than the impeller rotation frequency (Bakker *et al.,* 2000 and 2001).

5.5.4 Species Transport

When the sliding mesh model is used, species blending can be tracked along with the transient motion of the impeller. The species is normally introduced after the system has reached periodic steady state, but need not be. If an inflow boundary is to be used for species calculations after periodic steady state has been reached, it should be assigned the velocity of the species jet (using the background fluid) during the start-up period. One method that can be used to hasten the calculation during the start-up period is to start with a solution based on the MRF model, as is discussed in Section 5.3.1.

When the MRF model is used, transient species transport should be done with great care or avoided altogether. This is due to the fact that the velocities in the rotating frame, whether stored in the local or absolute frame, will give rise to erroneous behavior when they are used to convect a scalar in a transient manner. Graphical displays of the species distribution are suspect, even though the method can accurately capture the average species concentration as a function of time in the vessel as a whole.

5.5.5 Dispersed Phase Particle Tracking

The dispersed phase model, discussed in Section 2.2.2, allows for the coupled motion of a particle, bubble, or droplet stream with the fluid phase. When used with the sliding mesh model, the trajectories are computed in segments, with one segment per time step. The solver must ensure that the total time of each trajectory segment does not exceed the duration of the time step. If this condition is met, the particles can cross the sliding mesh interface without any incompatibility in the assumptions of either model. When combined with the MRF model, however, the implementa-

tion must be able to incorporate the particle motion in the rotating frame as well. While there are techniques for doing so, it is not clear that the results are meaningful in all reference frames. This combination of models should therefore be avoided.

VI

EVALUATING MIXING FROM FLOW FIELD RESULTS

While there are numerous options for simulating the fluid flow inside a stirred tank, the goal of the simulation is to learn about the various aspects of the flow field. On a simple level, this might include velocity vectors in one or more regions, path lines followed by infinitesmal fluid elements as they wind their way through the vessel, or the distribution of a tracer species after some period of time has passed, for example. On another level, the analyst might want to understand the power requirements for the motor, the time required to achieve adequate blending, or the fate of vortices trailing from the edges of the impeller blades. This type of information and more can generally be extracted from the CFD results, or can be obtained from auxiliary CFD calculations based on those results. To illustrate how, the following sections are presented that offer summaries and examples:

Section 6.1: Graphics of the solution domain
Section 6.2: Graphics of the flow field solution
Section 6.3: Other useful solution variables
Section 6.4: Mixing parameters

COMPUTATIONAL FLUID MIXING

These sections are designed to provide an overview of several of the methods used to make CFD analysis of mixing a meaningful endeavor.

6.1 Graphics of the Solution Domain

A stirred tank can be displayed in a number of ways to illustrate the relevant features of the vessel and its internals. These are described below.

6.1.1 Geometry Outline

Perhaps the simplest method for displaying the vessel is to draw an outline of the geometry. An outline consists of the features of the tank and internals, but little else. For 2D simulations either a side view or dotted lines (or both) can be used to represent the impeller and the location where the experimental data is applied to represent it. For 3D simulations modeled using the explicit geometry, all edges are shown.

6.1.2 Surfaces

In addition to the features shown in an outline, the surfaces can also be drawn. If solid surfaces are used for the tank, the viewer cannot see inside unless the viewpoint is through an opening in the side or the top (Figure 15). Alternatively, solid surfaces can be used for the internals and translucent surfaces can be used for the vessel walls (Figure 10.1). When displayed with lighting, the image can accurately convey the three dimensional nature of the entire geometry.
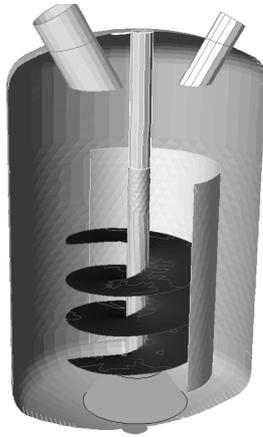
Figure 15
Geometry using
solid surfaces
with a cut in the
wall and top to
look inside.

6.1.3 Grids

For 2D simulations, a display of the grid (Figure 1.2) is an excel-
lent way of illustrating the potential level of accuracy in the solu-
tion. A coarse grid, despite a deeply converged solution, cannot
deliver accuracy on a scale any finer than the grid itself. A fine
grid, however, has the potential to deliver a much better resolved
flow field, assuming the solution is adequately converged. Most
grids are non-uniform, with fine and coarse grid regions. The
fine (and coarse) grid regions show the areas where the most (and
least) accurate details can be expected.

For 3D simulations, displays of the grid are more difficult to do
in a meaningful way. When the grid is structured, a single grid
plane can be displayed. In addition to showing the distortion in
the grid (if the grid plane is distorted), this type of display can
also show fine and coarse grid regions. For unstructured grids,
single grid planes do not exist. A cut through the solution domain
on, say, a surface of constant x-value, shows the cross section
through a number of cells, and is not necessarily helpful. A more

common approach is a display of the surface grid in 3D simulations (Figure 10.2). If the surface grid is fine (or coarse) in a region, the chances are good that the volumetric mesh in that region is fine (or coarse) as well.

6.2 Graphics of the Flow Field Solution

There are many ways to examine the flow field results, some of which are described below.

6.2.1 Vectors

Velocity vectors can be used to illustrate the magnitude and direction of the flow field throughout the solution domain. For 2D simulations, a plot of all velocity vectors gives an overall picture of the fluid behavior. For 3D simulations, a plot of all vectors in the domain is too crowded to be useful. Vectors need to be plotted on one or more planes or surfaces, instead, as is shown in Figure 11.2 and again in Figure 13. Note that the planes can be single grid planes (e.g. J = 10) or Cartesian grid planes (x = 3.5m). Surfaces can be planar or non-planar, such as a surface of constant temperature or a surface of constant radius. The important point is that for vector plots to be meaningful, the vectors (with length and orientation) need to be clearly visible, so the surfaces or planes used to plot them need be chosen accordingly.

6.2.2 Streamlines

In 2D simulations, a quantity called the stream function, ψ, is defined in terms of the density and gradients of the x- and y-components of the velocity, U and V. In terms of cylindrical coordinates, which are most appropriate for axisymmetric stirred tank models, the definition takes the form:

$$\rho U = \frac{1}{r}\frac{\partial \psi}{\partial r} \quad \text{and} \quad \rho V = -\frac{1}{r}\frac{\partial \psi}{\partial x} \tag{41}$$

where U and V are the axial and radial components of velocity. The stream function is constant along a streamline, a line that is everywhere tangent to the velocity field. When defined in the above manner, ψ incorporates a statement of conservation of mass. The difference between the stream function defined on any two streamlines is equal to the mass flow rate between the streamlines. Thus when a pair of streamlines has close spacing, the implication is that the velocity is greater than when the same pair has wide spacing, since the same amount of mass must pass through the space between the lines. Streamlines therefore have the ability to convey not only the relative movement of the flow, but the relative speed as well. In Figure 16, streamlines in a 2D simulation of a stirred tank are close as they pass through the impeller, where the boundary conditions are imposed and the flow speed is high. They are also close along the outer wall, but are more widely spaced elsewhere, where the flow recirculates in a larger area at a much slower speed.
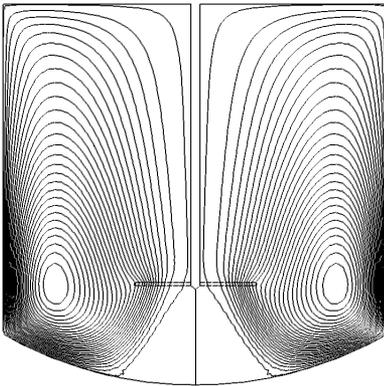
Figure 16
Streamlines for a 2D simulation of a pitched-blade impeller with a single recirculation zone showing high and low speed regions.

6.2.3 Path Lines

Since the stream function is only defined for 2D flows, an alternative method is needed to visualize 3D flows in the same manner. Path lines can be used for this purpose. Path lines follow the trajectories that would be followed by massless particles seeded at any location within the domain. These particles move with the flow field, and leave behind tracks in one form or another that allow the flow field to be visualized. In Figure 17, path lines are used to illustrate the flow through a static mixer. Path lines can be drawn as simple lines or as tubes, ribbons, or a series of dots. They can usually be colored by problem variables, such as temperature. When colored by time, they give information on residence time if inflow and outflow of fluid are involved.
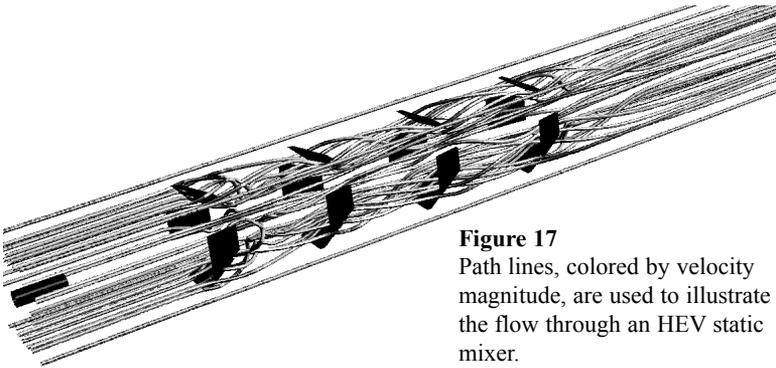
Figure 17
Path lines, colored by velocity magnitude, are used to illustrate the flow through an HEV static mixer.

6.2.4 Contours

Contours are lines where a chosen variable has a constant value. The streamlines illustrated in Figure 16 are actually contours of stream function, since ψ is constant on each of the lines shown. In addition to line contours, filled contours, plotted on an entire 2D domain or on a surface in a 3D domain, are also very useful for showing the maximum and minimum values as well as local

gradients. In Figure 18, contours of a tracer species are shown on a cross section through a 3D domain.
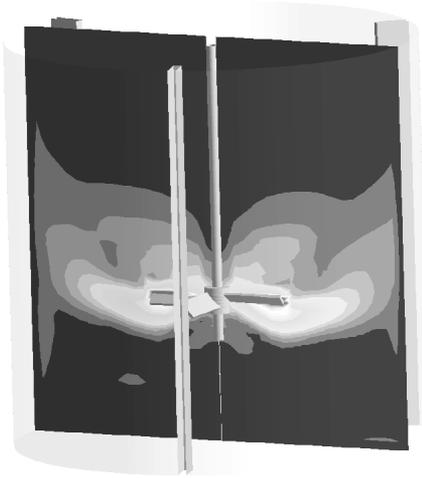
Figure 18
Filled contours of a tracer species shown on a planar surface in a 3D domain.

6.2.5 Isosurfaces

Isosurfaces in 3D flow fields are analogous to contour lines in a 2D flow field. These three dimensional surfaces are constructed in such a way that a particular variable has a constant value everywhere on it. If the isosurface has a constant value of the Cartesian coordinate x, for example, it is planar. If it has a constant value of velocity in a stirred tank, it is complex in shape and can have several disconnected regions. Isosurfaces of this type can be plotted as solid surfaces with lighting (Figure 19), to convey the three dimensional nature of the variable distribution. They can also be used to plot contours, showing how one variable changes as another one is held fixed.
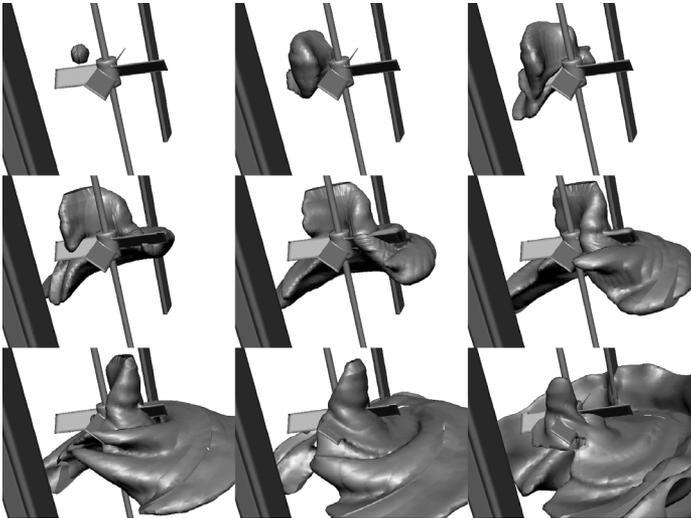
Figure 19
The dispersion of a tracer in a stirred tank. A blob of tracer is injected
at time zero, and its dispersion is shown after 1/4, 1/2, 3/4, 1, 1-1/4,
1-1/2, 1-3/4, and 2 impeller revolutions, respectively.

6.2.6 Particle Tracks

Whenever the discrete phase model is used (Section 2.2.2), parti-
cle tracks can be used to illustrate the trajectories of the particles,
bubbles, or droplets. Trajectories usually can be displayed in a
number of ways. For example, lines can be colored by the time
of the trajectory or temperature of the particle itself. In addition
to lines, ribbons and tubes can generally be used. The tracks can
be computed and displayed using the mean fluid velocities, or in
the case of turbulent flows, using random fluctuations in the
mean fluid velocities as well. These so-called stochastic tracks
often give a more realistic picture of the extent to which the par-
ticles reach all corners of the solution domain than do tracks com-
puted from the mean velocities alone.

6.2.7 Animations

Animations can be created from groups of image files that follow a process from beginning to end, or during some period of operation. They can also be used to follow the motion of massless particles in a steady-state flow field. Numerous postprocessing packages are commercially available for the creation of animations, and many CFD packages have built-in functionality to do so as well.

Types of Animations

Some examples of how animations can be used for displaying flow field results are listed below. In general, anywhere from twenty to hundreds of images, or frames can be created and concatenated, or joined together to form the animation. The content of these images is a function of whether the simulation is steady-state or time-dependent, and on what the display goals are intended to be. In general when creating animations, care should be taken to avoid incorporating too much information into a single image, since some of this information will inevitably be lost on the viewer.

Time-Dependent Simulations

For time-dependent flow fields, images should be made at uniform time intervals for the purpose of creating a meaningful animation. Examples of time-dependent animations include

- contours of tracer concentration on a single plane during blending
- velocity vectors on a plane during a turbulent simulation modeled using large eddy simulation
- gas from a sparger filling a stirred tank or a bubble column
- lifting and suspension of solids off the vessel floor in a stirred tank

85

· isosurfaces of vorticity trailing from a rotating impeller in a sliding mesh model

Path Lines

Path lines are normally created by a simultaneous calculation and display of trajectories, using the problem geometry and flow field data. To generate an animation of evolving path lines, frames of the trajectories at intermediate stages need to be created and stored. To do this, a total time for the animation needs to be determined along with a number of frames to be made. Tools are available in most visualization packages to generate the intermediate frames based on these inputs, using dots, lines, or other geometric entities. The intermediate frames can be written to files in one of a number of available formats. When played in succession, the concatenated frames will mimic the display that is generated by the original visualization software.

Moving Slice Planes

One method of illustrating the change in a variable throughout a 3D domain is through the use of animated slices. For example, in a stirred tank, the velocity field at different angular locations - from one impeller blade to the next or from one baffle to the next - might be of interest. Planar slices at equal angle intervals can be used for each frame, on which either contours or in-plane velocity vectors are displayed. A series of axial slices is another useful way to examine the change in a variable from one end of a mixer to another. This type of animation is particularly useful for static mixers.

Moving Iso-Surfaces

When injecting a tracer, one method of following its evolution is

by animating isosurfaces of the tracer mass fraction. The animation is made most effective if the same numerical value is chosen for each frame. The value should be small in magnitude so that the expanding surface at later times can be captured. If the data for all times exists prior to the creation of the images, the data for the first and last times should be used to plan the best isosurface value to track for the duration of the process. When plotted as a solid surface with lighting, the three-dimensional nature of the isosurface is easy to discern and the effect makes for an exciting and informative animation.

Moving Impeller Blades

In stirred tank animations, it is always helpful if the motion of the impeller can be animated as well. This is possible in sliding mesh simulations, where the changing position of the impeller can be captured in successive frames. Some animation software can extract this motion from MRF simulation data, where the rotation speed of the impeller is known. Based on the time interval between frames, the impeller is advanced by a computed angle in each display created. When the frames are animated, a continuous motion of the impeller can be seen, along with other animated variables, such as path lines or changing contours on a stationary surface.

Moving Viewpoint

For steady-state external flows, animations based on a moving viewpoint are popular. These animations can also be used to illustrate the complex geometry of a system, such as a stirred tank and its internals. Beginning with a distant view, the camera can approach the object and peer inside to get close-up views of the components.

COMPUTATIONAL FLUID MIXING

Creating Animations from a Collection of Images
Numerous commercial software packages are available today for creating an animation from a collection of images. Different image file formats are available for this purpose. Once the images have been concatenated to form the animation, tools are available in most animation packages to set the speed of the animation. A choice of about 0.05 seconds between frames usually results in a smoothly playing animation, but this also depends on the number of frames and the capabilities of the computer. It should be noted that the time interval mentioned here refers to the playing time, not the physical time between the data used for each frame display.

6.3 Other Useful Solution Variables

In the previous section, methods of plotting several common solution variables, such as velocity, stream function, and species concentration were discussed. Plots of turbulent kinetic energy and dissipation are also of interest in turbulent flows, especially if other processes such as chemical reactions are to take place. In multiphase flows, the volume fraction of the phases is the most useful tool to assess the distribution of the phases in the vessel. In this section, three additional quantities are reviewed that are derived from the velocity field. These can provide a deeper understanding of the flow field than plots of the velocity alone.

6.3.1 Vorticity

Vorticity, a vector quantity, is a measure of the rotation of the fluid. In terms of a fluid element, a non-zero vorticity implies that the element is rotating as it moves. The vorticity is defined as the curl of the velocity vector, u:

$$\xi = \nabla \times \mathbf{U} \tag{42}$$

Vorticity can be defined in both 2D and 3D flows. In 2D flows, the direction is normal to the plane of the simulation. This means that for a 2D, axisymmetric simulation of flow in a stirred tank, the vorticity is always in the circumferential direction.

$$\xi_\theta = \frac{\partial U_x}{\partial r} - \frac{\partial U_r}{\partial x} \tag{43}$$

In 2D simulations, positive values indicate counter clockwise rotations, while negative values indicate clockwise rotation. In a 3D simulation, vorticity can take on any direction, and plots of vorticity magnitude, rather than the individual components, are often the most helpful. The units of vorticity are sec^{-1}, the same as those used for shear rate. In Figure 20.1, contours of vorticity are shown for a 2D flow in a stirred tank with velocity vectors superimposed on the display. White regions have a maximum
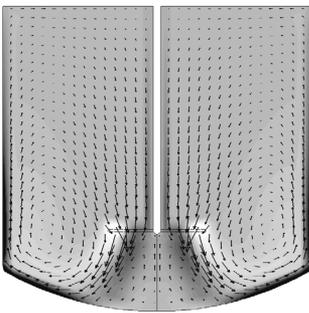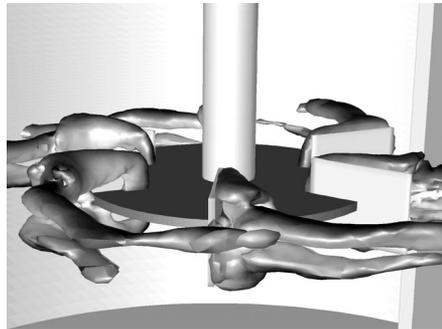
20.1   20.2

Figure 20
Contours of vorticity in a 2D simulation with superimposed velocity vectors (20.1) and isosurfaces of vorticity magnitude behind a Rushton turbine (20.2).

positive value and black regions have a maximum negative value. Regions where steep normal gradients in the velocity occur (near the outer walls and impeller) are shown to have the maximum values of vorticity, as expected. The fact that the vorticity is pos-

itive near the impeller and negative near the wall indicates simply that the direction of the curl is opposite in these two regions. In Figure 20.2, isosurfaces of constant vorticity magnitude in a 3D simulation show the trailing vortices behind a Rushton impeller. The simulation was performed using the LES turbulence model.

6.3.2 Helicity

The helicity is defined as the dot product of the velocity vector with the vorticity vector:

$$\mathbf{H} = \mathbf{U} \bullet \boldsymbol{\xi} = \mathbf{U} \bullet (\nabla \times \mathbf{U}) \tag{44}$$

Clearly, the helicity has a value of zero in 2D simulations. In 3D simulations, it gives an indication of how well the local rotation of a fluid element is aligned with the velocity of the element. It is useful for illustrating longitudinal vortices, or spiral motion, as is often found in vortex cores. In Figure 21, isosurfaces of helicity are used to depict the longitudinal vortices generated in the Kenics static mixer described in Section 7.10.
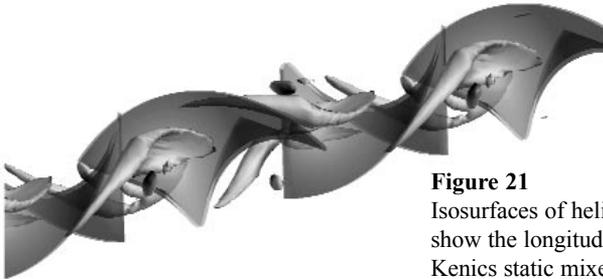
Figure 21
Isosurfaces of helicity are used to show the longitudinal vortices in a Kenics static mixer.

6.3.3 Rate of Deformation

The rate of deformation, or strain rate tensor is a collection of terms that together describe the complete deformation of a fluid

element in motion. The deformation can be the result of linear strain, which gives rise to a linear deformation or stretching of the element, and shear strain, which gives rise to an angular deformation or change in shape of the element. The symmetric tensor has components of the generalized form:

$$S_{ij} = \frac{1}{2}\left(\frac{\partial U_i}{\partial x_j} + \frac{\partial U_j}{\partial x_i}\right) = S_{ji} \qquad (45)$$

While the tensor components themselves offer little insight into the behavior of the flow field, functions of the tensor components often do. In terms of the Cartesian coordinates *x, y,* and *z*, the diagonal terms are:

$$S_{xx} = \frac{\partial U_x}{\partial x} \qquad S_{yy} = \frac{\partial U_y}{\partial y} \qquad S_{zz} = \frac{\partial U_z}{\partial z} \qquad (46)$$

Each of these terms represents a linear strain rate, or rate of elongation of the fluid element in each of the three coordinate directions. The sum of these diagonal terms is the trace, or first invariant of the tensor. For incompressible fluids, this quantity is always zero, since the volume of the fluid element must be conserved.

In addition to the trace, another quantity, often referred to simply as the strain rate, is of interest. The strain rate, taken from the modulus of the tensor, is a positive-definite representation of all possible components of the strain rate tensor. It is used to determine the viscosity in strain-dependent non-Newtonian fluids, and is also helpful as a reporting tool for mixing applications. In particular, regions with high strain rate play an important role in liquid dispersion.

COMPUTATIONAL FLUID MIXING

6.4 Mixing Parameters

Parameters that are used to characterize stirred tank flows and mixing processes in general can be computed by correlations that can be found in the literature. In many cases, these parameters can also be computed from the CFD results. Examples of how to compute some of these parameters are given below.

6.4.1 Power Number

The power number is a dimensionless parameter that provides a measure of the power requirements for the operation of an impeller. It is defined as

$$N_P = \frac{P}{\rho N^3 D^5} \tag{47}$$

In the above expression, P is the power applied to the impeller of diameter D, ρ is the density, and N is the impeller rotation speed, in Hz. Correlations are available that provide the dependence of N_P on the Reynolds number. Thus if CFD is not available, the power requirements can generally be obtained from one of these correlations. The correlations can break down, however, if they do not address the D/T or C/T ratios of single impellers or the presence and spacing of multiple impellers. In such cases, CFD results can be used to compute N_P, or simply, the power requirements.

The power delivered to the fluid is the product of the impeller speed, $2\pi N$, in radians/sec, and torque, τ, which is obtained by integration of the pressure on the impeller blade:

$$P = 2\pi N\tau \tag{48}$$

Reports are usually available for the torque delivered to the fluid

by the impeller. In some cases, reports of power or even power number can be obtained from the software.

Integration of the Dissipation

In principle, the power delivered to the mixer is equivalent to that lost, or dissipated in the fluid. An integration of both the viscous and turbulent dissipation throughout the volume should, therefore, be an acceptable way to compute the power draw. The dissipation rate predicted by the various turbulence models can vary significantly, however, and there is no guarantee that the turbulence model that gives the best flow pattern prediction also gives the best dissipation rate prediction. For laminar flows, even with a refined mesh near the impeller blades, CFD can have difficulty predicting viscous dissipation in a satisfactory manner. For this reason, the best method for extracting the power drawn by the impeller is by calculation of the torque on the blade surfaces.

6.4.2 Flow Number

The flow number is a measure of the pumping capacity of an impeller. Different measures for pumping capacity exist, but the flow number is widely used. It is defined as:

$$N_Q = \frac{Q_\ell}{ND^3} \tag{49}$$

In this expression, Q_ℓ is the flow rate produced by the impeller. The subscript is used to ensure that the flow rate for the liquid phase alone is used in the calculation. To compute Q_ℓ for an impeller, a surface needs to be created for the discharge region. This surface would be circular for an axial flow impeller and a section of cylinder wall for a radial flow impeller. By integrating the total outflow through this surface, the flow rate, Q_ℓ, and subsequently the flow number, N_Q, can be obtained.

93

6.4.3 Evaluating Mixing Time

A transient blending calculation is the best method for determining the time required to achieve a certain level of blending. When a tracer is added to a fluid in a mixing tank, the transient calculation can be done exclusive of the flow field calculation if the properties of the tracer and background liquid are identical. When this is the case, a steady-state calculation can be performed for the background liquid using either experimental data or the MRF method, although care should be exercised when using the latter, as it discussed in Section 5.5.4. If inflow and outflow ports are to be used, the simulation of the background liquid alone should include the inflow boundary conditions for velocity that will ultimately be used for the tracer. Once the flow field for the background fluid is satisfactorily converged, the tracer can be introduced. Since the mixture fluid properties will not change with the addition of the tracer, the transport equations for momentum, continuity, and turbulence can be disabled while the transient species calculation takes place. The transient solution of this single scalar equation will be robust (since it is not coupled to other variables that are in a state of change) and economical, advancing rapidly with few iterations required each time step. Averages of the tracer concentration, along with standard deviations, can be computed throughout the vessel to determine when the tracer has become fully blended.

There are two exceptions to the use of the method described above, in which the flow field calculation can be disabled during the species calculation. First, if the sliding mesh model is used, the flow field data is required for each time step, so it is not possible to disable the flow field calculation to perform the species transport calculation. Second, if the tracer is to be added through

an inlet or dip tube for a finite period of time, after which the inlet flow is disabled, the calculation of the flow field should resume at that time, especially if the inlet delivers a jet of significant momentum to the vessel.

6.4.4 Information from LES Simulations

Large eddy simulations are transient simulations designed to capture the fluctuations that are the result of turbulent eddies. For this reason, LES images and animations have the potential to capture small and large scale activity that would otherwise be averaged to zero with a RANS turbulence model. Some of the small scale activity includes the birth and death of eddies or small vortices. Some of the large scale activity includes low frequency instabilities in stirred tanks. A common way to visualize the turbulent structure present in LES simulations of mixers is by animating vectors or isosurfaces of vorticity magnitude.

COMPUTATIONAL FLUID MIXING

VII

APPLICATION EXAMPLES

To illustrate the successful application of CFD to many types of process equipment, a number of examples are presented in this chapter, as listed below.

Section 7.1:   Blending in a Stirred Tank Reactor
Section 7.2:   Chemical Reaction in a Stirred Tank
Section 7.3:   Solids Suspension Vessel
Section 7.4:   Fermenter
Section 7.5:   Industrial Paper Pulp Chests
Section 7.6:   Ozone Decomposition in a Fluidized Bed
Section 7.7:   Bubble Columns
Section 7.8:   Twin-Screw Extruders
Section 7.9:   Intermeshing Impellers
Section 7.10: Kenics Static Mixer
Section 7.11: HEV Static Mixer
Section 7.12: LDPE Autoclave Reactor
Section 7.13: Impeller Design Optimization
Section 7.14: Helical Ribbon Impeller
Section 7.15: Stirred Tank Modeling Using LES

Unless otherwise noted, these simulations were performed with software from Fluent Inc.

COMPUTATIONAL FLUID MIXING

7.1 Blending in a Stirred Tank Reactor

Mixing time correlations for stirred tank reactors are available, but these are often difficult to extend outside the experimentally studied parameter range. One advantage of CFD is that it can be used to evaluate industrial size equipment or equipment for which no correlations are available. A comprehensive evaluation of the accuracy of mixing time predictions using CFD was presented by Oshinowo *et al.* (1999). The main conclusion drawn was that although unsteady tracer dispersion predictions based on a steady state flow field are acceptable, the accuracy of the predicted mixing time is greatest when the mixing simulation is based on a time dependent calculation, using the sliding mesh model. For the latter method, either the LES model or a standard turbulence model such as RSM may be used.

Figure 19 shows an example of the dispersion of a chemical tracer in a stirred tank. A standard pitched blade turbine is used to mix two water-like materials. The neutrally buoyant tracer is injected at time zero as a blob above the impeller, as shown on the top left in the figure. The flow field is calculated using the sliding mesh model, and the dispersion of the tracer is derived from the flow field. For this particular example, the LES turbulence model is used, although good results have also been obtained with other turbulence models. The blob is stretched and the chemical is mixed with the rest of the fluid over time. It is interesting to see that despite the fact that there are four impeller blades and four baffles, the concentration field is not symmetric because of the off-axis injection. The consequence is that the full tank needs to be modeled instead of a ninety degree section.

7.2 Chemical Reaction in a Stirred Tank

The blending of chemical reactants is a common operation in the chemical process industries. When a competitive side reaction is present, the final product distribution is often unknown until the reactor is built. This is partly because the effects of the position of the feed stream on the reaction byproducts are difficult to predict. In this example from Bakker and Fasano (1993), the product distribution for a pair of competing chemical reactions is calculated with CFD and compared with experimental data from the literature. The model used here is a slightly modified version of the standard Magnussen model discussed in Section 2.2.1.

The following competitive-consecutive reaction system was studied:

$$A + B \xrightarrow{K_1} R$$

(50)

$$B + R \xrightarrow{K_2} S$$
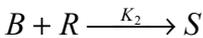
This is the reaction system used by Bourne *et al.* (1981) and Middleton *et al.* (1986). The first reaction is much faster than the second reaction: K_1 = 7300 m³/mole-s vs. K_2 = 3.5 m³/mole-s. The experimental data published by Middleton *et al.* were used to determine the Magnussen model constants. Two reactors were studied, a 30 liter reactor equipped with a D/T=1/2 Rushton turbine and a 600 liter reactor with a D/T=1/3 Rushton turbine. In the CFD analysis, a converged flow field was computed first for each reactor, using experimental data for the impeller boundary conditions. The reactants A and B were then introduced to the tank on an equimolar basis. The reactant A was assigned a weak, but uniform concentration throughout the vessel. The reactant B

was added in a high concentration in a small region. The calculation of the flow field variables was disabled after the addition of the reactants, and the species calculations alone were performed. Once the solution converged, the product distribution X_s was calculated using:

$$X_s = \frac{2C_s}{C_R + 2C_s} \qquad (51)$$

In the reaction model used here it was assumed that small scale mixing only affected the first reaction and that once this reaction had occurred, the species were locally well mixed. As a result, small scale turbulent mixing did not affect the second reaction. This was achieved by using different values of the Magnussen model constants for the two reactions.

Figure 22 shows a comparison between the experimental data from Middleton *et al.* and the CFD predictions for both reactors. The product distribution, X_s is plotted as a function of impeller speed, in RPM. This graph shows that the model predicts the effects of scale and impeller rotational speed correctly, and is usually within 10% of the experimental results.
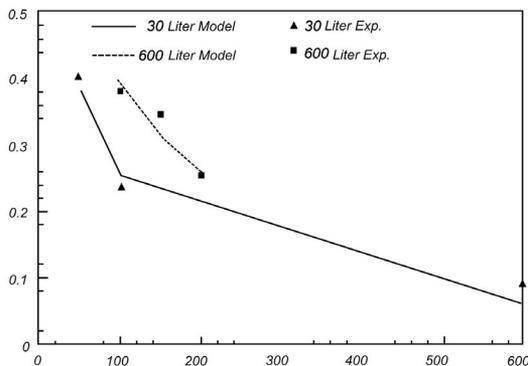
Figure 22
The product distribution, X_s as a function of impeller speed (RPM) for two vessels of different size, with the second reactant being added in the outflow of the impeller. Model predictions compared with the data from Middleton *et al.* (1986).

The effect of the inlet position of the feed stream on the formation of the byproduct, S, was also studied. Figure 23 shows values of X_s for various feed locations. X_s varies only slightly when the inlet is located in the fluid bulk. However, when the feed is injected directly above the impeller, such that the feed stream immediately passes through the highly turbulent impeller zone, local mixing is much faster and does not limit the rate of the first reaction. As a result there is less reaction byproduct, S, and the final X_s is only 50% of what it would be if the feed were located away from the impeller. This qualitatively agrees with the experimental results of Tipnis *et al.* (1993), who used a different set of reactions and tank geometries but also found that injection near the impeller resulted in a lower X_s than injection farther away from it. The relative differences found by Tipnis *et al.* are similar to those shown in this example.
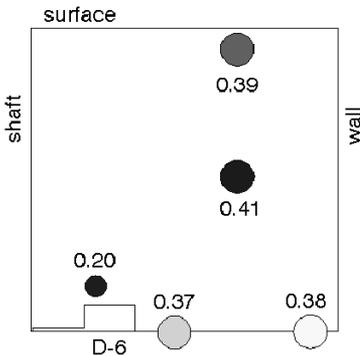
Figure 23
The product distribution X_s as a function of feed location for a 600 liter vessel with a Rushton turbine operating at 100 RPM. The product distribution is reduced by about a factor of two when the feed is positioned directly above the impeller.

7.3 Solids Suspension Vessel

Stirred tanks for solids suspension applications have traditionally been designed using the just-suspended impeller rotational speed, N_{JS}. Although much work about solids suspension has been published, most of it concentrates on providing correlations for the just-suspended speed. Attempts to develop mathematical

models for the solids suspension process are often based on the total power draw of the impeller, or the average liquid velocity in the tank, without taking local effects into account. The effect of the flow pattern on the spatial distribution of the solids has received relatively little attention. It is now known that the solids spatial distribution is strongly affected by the number of impellers, their location, and certain flow transitions. When either the D/T or C/T ratios are too large, a flow transition with reversed flow at the vessel base may occur. This results in an undesired increase in the power needed to suspend the solids, or more simply, N_{JS}.

Adding a second impeller typically has a very small effect on the just-suspended speed. In multiple impeller systems, zoning occurs when the impeller separation is too large. The most efficient solids mixing occurs just before the flow between the impellers separates. Unfortunately, designing on the basis of the just-suspended speed or on the basis of power consumption does not necessarily lead to an optimum multiple impeller system.

Figure 24 shows a comparison of the solids distribution for a single (left) and a dual (right) impeller system in a tall stirred tank, modeled using experimental data for the impellers, and the Eulerian granular multiphase model for the solids suspension (Oshinowo *et al.*, 2000). The results on the left show that in a tall tank equipped with a single impeller, the solids do not move up higher than about half the liquid level. When a second impeller is added, however, such that one long flow loop is formed, the solids reach the level of the second impeller, as shown on the right. When the second impeller is placed too far above the first impeller and zoning occurs, the solids do not reach the upper

impeller (not shown, see Bakker *et al.*, 1994). From the differences between the solids suspension performance of these two two-impeller systems it can be concluded that consideration of the just-suspended speed or power draw alone does not necessarily lead to the best design. The impeller system has to be designed so that it provides the optimum flow pattern for the suspension duty to be performed. To design such a system, the effects of the flow pattern on the solids distribution must be taken into account. Computer simulation provides an excellent tool for this purpose.
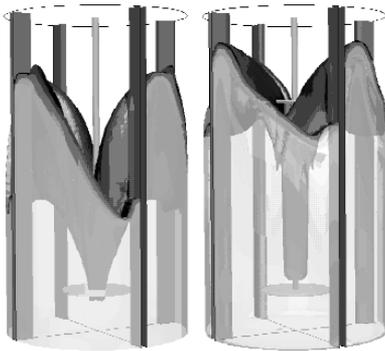
Figure 24
Solids suspension in a tall vessel. The solids distribution with a single impeller is shown on the left, and with a dual impeller system is shown on the right.

7.4 Fermenter

Large scale fermenters are used to make such products as yeast, vitamin C, xantham-gum, citric acid, and penicillin, for example. Fermentations are usually carried out in tall vessels with multiple impeller systems. Air is sparged in at the bottom, to provide the micro-organisms in the vessel with a supply of oxygen. It is important that the mixer disperse the gas into fine bubbles, a condition that is required to ensure good mass transfer from the air to the broth.

Figure 25 shows the results of a gas dispersion simulation of a fermenter. The fermenter is equipped with a radial flow CD-6

impeller with concave blades at the bottom, and three down pumping HE-3 impellers on top. The vessel has no baffles, but is equipped with twelve sets of eight cooling coils, that also act as swirl suppressors. Flow field simulations can be performed to design the impeller system such that there is sufficient liquid movement around these coils.

Gas Volume Fraction $3k_l a$ (1/s)   30(Bubble Size) (m)
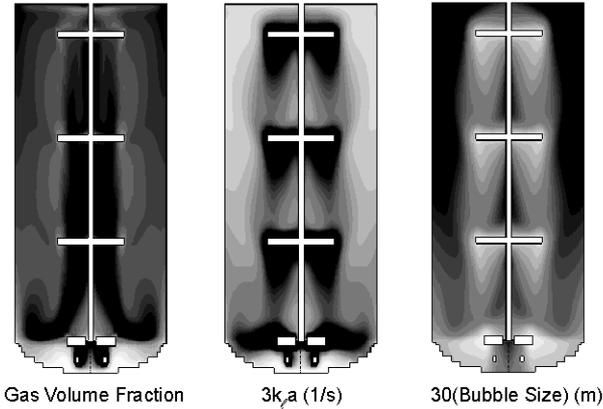
Figure 25
The picture on the left shows the local gas volume fraction, the picture in the center shows the local mass transfer coefficient $k_l a$, and the picture on the right shows the local bubble size. The bubble size is smallest near the impellers (light) and increases away from the impellers due to coalescence. The mass transfer coefficient is highest near the impellers, because this is where the bubble size is small (leading to a large interfacial area), and where the turbulence intensity is high (leading to fast surface renewal around the bubbles).

The gas-liquid simulations shown here were performed with software developed by Bakker (1992), which contains models for gas dispersion, bubble coalescence and break-up, and interphase mass transfer. The local gas volume fraction is shown on the left. The local mass transfer coefficient $k_l a$ (with values multiplied by 3) is shown in the middle, and the local bubble size (with values multiplied by 30) is shown on the right. All figures share the

104

same scale from 0 to 0.3 (which is why the mass transfer coefficient and local bubble size distributions are multiplied by a factor). The bubble size is smallest near the impellers and increases away from them, due to coalescence. The mass transfer coefficient is highest near the impellers, where the bubble size is smallest (leading to a large interfacial area), and where the turbulence intensity is highest (leading to fast surface renewal around the bubbles). The stair-stepped representation of the curved vessel bottom was necessary using the software available at the time of this simulation. The need for rectangular cells has since become obsolete with the introduction during the past several years of boundary-fitted cells and unstructured grids.

7.5 Industrial Paper Pulp Chests

One example of a difficult mixing problem is found in the paper industry. Paper pulp, which is a suspension of thin, flexible fibers, exhibits a very complex rheology. As a result, multiple flow regimes are found in paper pulp storage tanks, or chests, which can be rectangular or cylindrical in shape. Laminar flow is common in some parts of the chest, while turbulent flow is common in others. The bottom of the chest is usually filleted, and either sloped, curved, or both. Although paper pulp chests are sometimes equipped with top entering agitators, the preference in the paper industry is to use side-entering agitators.

The rheological properties of fiber suspensions are discussed in a paper by Gullichsen (1985). The fiber suspension initially behaves as a non-Newtonian fluid with a yield stress, τ_y. Above τ_y the paper pulp behavior is non-Newtonian. When the shear stress exceeds a second threshold value, τ_d, the fiber network structure is disrupted and the suspension behavior is similar to

that of a turbulent Newtonian fluid. As a result of this rheological behavior, fiber suspensions are extremely difficult to agitate. To provide motion throughout the whole tank, the shear stress has to exceed the yield stress everywhere in the fluid. Since gradients in the shear stresses can be expected, there will be regions in the fluid where the fiber network structure is disrupted and the flow is turbulent. At the same time the flow may be laminar or even stagnant in other parts of the chest. This combination of turbulent flow and laminar flow of a non-Newtonian fluid makes paper pulp storage chests difficult to model with CFD.

In an effort to address this problem, Bakker and Fasano (1993) developed a model for the flow of paper pulp. To model the complex fiber suspension, the following method was used. For every computational cell, the computations are first performed as if the flow were turbulent. A check is then done to see if the total shear stress is indeed larger than τ_d. If this condition is not met, the calculations for that particular cell are repeated as if the flow were laminar. The local apparent viscosity is then calculated from the experimental shear stress vs. shear rate curves and the local shear rate. The model has since been successfully used to predict the flow patterns in large industrial chests where zones with turbulent mixing, laminar mixing, and stagnant regions can easily be located.

Figure 26 shows the flow pattern in one example of a stock chest for mixing and storage of paper pulp. The agitator is modeled using experimental data. The flow pattern with a solution of 1% pulp is shown on the left. The figure on the right shows how the flow pattern changes when the concentration is increased to 5% and the same impeller speed is used. The results show that more power must be applied to maintain adequate flow conditions

when the pulp concentration is increased. The model is an excellent tool for the optimization of agitators for large industrial storage chests, and has been successfully used over the years for many different paper pulp applications.

1% pulp   5% pulp
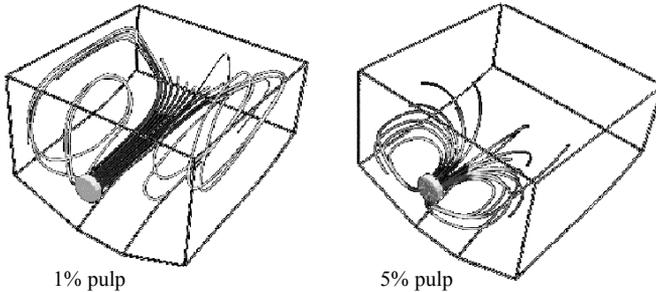
Figure 26
This figure shows the flow pattern in a stock chest for mixing and storage of paper pulp. The image on the left shows the flow pattern with a solution of 1% pulp. The image on the right shows how the flow pattern changes when the concentration is increased to 5%.

7.6 Ozone Decomposition in a Fluidized Bed

Fluidized beds are used in the chemical industry for catalytic reactions. Bed conversion refers to the process by which the passage of one material through the bed is converted to another during transit. Design of the system for optimum conversion strongly depends on knowledge of both hydrodynamics and chemical reactions. In this example, the Eulerian granular multiphase (EGM) model is used to capture the hydrodynamics, and a special reaction model is used to predict the decomposition of ozone as it passes through a cylindrical fluidized bed. The vessel is 0.23 meters in diameter and 0.25 meters high, and is simulated using an axisymmetric grid of about 8000 computational cells. At rest, the bed is 0.12 meters high, and contains catalyst particles (sand impregnated with iron oxide) 117 microns in diameter. Two gas

107

phase species are used in the model, ozone and oxygen. Ozone gas enters from inlets at the bottom of the bed. The gas lifts and separates the particles in the bed, allowing for better interaction between the ozone and particle surfaces. The iron oxide causes the ozone molecule, O_3, to give up an oxygen atom and leave behind an oxygen molecule, O_2. A mixture of ozone and oxygen exits through the upper surface of the column.

The decomposition reaction is first order for the two gas species:

$$O_3 \longrightarrow 1.5\ O_2$$
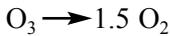
The decomposition rate is expressed as

$$K = 1.57\ a\ [O_3],$$

where a is the volume fraction of the catalyst and $[O_3]$ is the concentration of ozone. A user-defined subroutine is used to calculate the reaction rate and ensure that the reaction takes place in the bed region only. The calculations are done for inlet gas velocities in the range from 4 to 14 cm/s.

Figure 27 shows the gas volume fraction one second after the flow is initiated. The flow field is the same whether the reaction in the gas phase is taking place or not. The bubbles are formed near the bottom of the bed and migrate upwards, lifting the surface before breaking through it. The bubble shape and size are grid dependent. On coarser meshes, the bubbles are fewer in number and rounder. On finer meshes, the bubbles are denser and more irregular. The number of bubbles has a significant impact on the conversion. The more bubbles in the domain, the higher

the conversion. While some large bubbles stand out, the bed itself is filled with small bubbles to a greater or lesser degree. A bed filled with bubbles in this manner is the desired hydrodynamic state for optimum conversion.
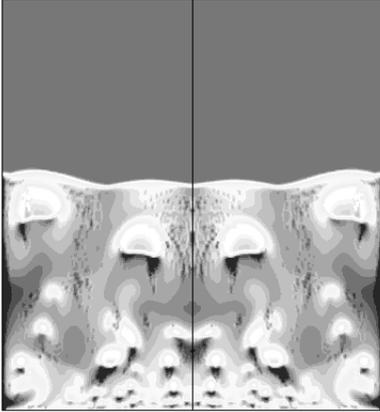
Figure 27
The fluidized bed after one second of operation.

In Figure 28, the conversion curve (top) and gas holdup (bottom) as functions of the gas velocity are plotted. The gas holdup is defined as the ratio of the gas in the bed to the total volume of the bed. The curve shows that the gas holdup increases with gas velocity up to a point, after which saturation occurs. This is because at the low end, the increasing gas velocity forces the bed to lift more. When saturation occurs, the bed can no longer rise and hold additional gas. The conversion curve is a plot of C_{out}/C_{in} for ozone. It is plotted along with data from Fryer *et al.* (1976), and good agreement is in evidence. The results follow the trends in the gas holdup. At low gas speeds, the residence time is long, allowing more time for the ozone to come into contact with the particles. Conversion is high, so C_{out}/C_{in} is small. At high speeds, the residence time reduces, and conversion is poorer, tending toward a constant value.

109
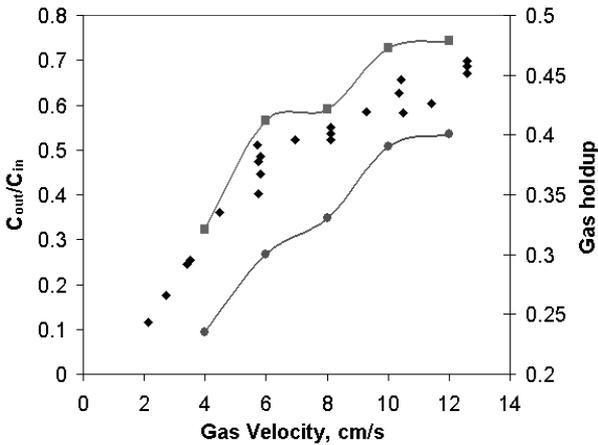
Figure 28
Gas holdup (lower curve) and (1-conversion) (upper curve) as functions of superficial velocity. Experimental values for (1-conversion) are also shown.

7.7 Bubble Columns

Bubble columns are contactors in which a discontinuous gas phase in the form of bubbles moves relative to the continuous liquid phase. As reactors, they are used in a variety of chemical processes, such as Fischer-Tropsch synthesis, manufacture of fine chemicals, oxidation reactions, alkylation reactions, effluent treatment, coal liquefaction, fermentation reactions, cell cultures, and the production of single cell proteins. The principal advantages of bubble columns are the absence of moving parts, leading to easier maintenance, high interfacial areas and transport rates between the gas and liquid phases, good heat transfer characteristics, and large liquid holdup, which is favorable for slow liquid phase reactions. The complex processes in bubble column reactors affect the reactor operation and performance. In industrial operation, the turbulent two-phase flow determines the transient and time-averaged values of gas holdup distribution, the extent of

110

liquid phase backmixing, the gas-liquid interfacial area, the gas-liquid mass and heat transfer coefficients, the bubble-size distributions, the bubble coalescence and redispersion rates, and the bubble rise velocities. The lack of complete understanding of the fluid dynamics makes it difficult to improve the performance of a bubble column reactor simply by judicious selection and control of the operating parameters.

CFD is now being used to better understand the interaction of these and other variables. Both bubbly and churn-turbulent bubble column flow regimes can be simulated (Sanyal *et al.*, 1999). Figure 29 shows the results of a time dependent simulation of the velocity field and gas holdup profile in a 3D simulation of a cylindrical bubble column. The image in the center shows a surface at which the volume fraction of gas is 30%. Inside the surface, the volume fraction of gas is higher. The plot on the left shows the velocity vectors on this surface. The plot on the right shows the liquid velocity vectors in a plane through the center of the column.

Figure 29
Simulation of the time dependent velocity field and gas holdup profile in a bubble column. The plot in the center shows a surface at which the volume fraction of gas is 30%. Inside the surface, the volume fraction of gas is higher. The plot on the left shows the velocity vectors on this surface. The plot on the right shows the liquid velocity vectors in a plane through the center of the column.
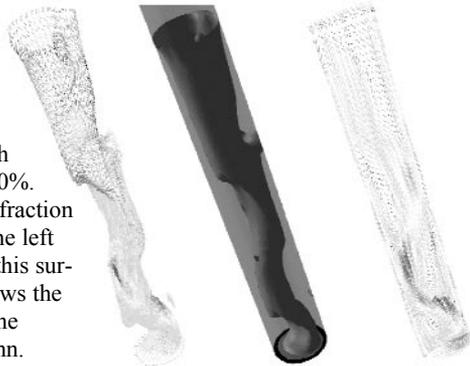
CFD results for bubble column flow have been validated against experimental data in a number of studies. See Vasquez *et al.*

111

(2000), for example. Good agreement is obtained when the results are compared with experimental data obtained via the non-invasive, computer automated radioactive particle tracking experimental technique, described in this paper.

Simulations such as these can be used to predict gas holdup, mass transfer rates, mixing rates, and process performance of bubble columns. One of the advantages of CFD over the use of traditional bubble column design correlations is that the CFD models also apply to situations outside the range for which experimental data was obtained.

7.8 Twin-Screw Extruders

The twin-screw extruder is one of the most widely used tools, not only in the plastics and rubber industry but also in other areas such as food processing. Single- and twin-screw extruders are used to melt, convey, compress, and mix the different compounds involved in any given process, and these steps can considerably affect the quality of the final product. This explains the large interest in screw analysis and, more specifically, the numerous attempts to model twin-screw extruders through numerical simulations. The challenges involved in such simulations (moving parts, thermal behavior, difficult meshing and remeshing tasks, and partial filling, for example) often lead to many simplifications of the actual problem.

In order to ease the set up of a three-dimensional unsteady twin-screw extruder, a technique referred to as mesh superposition, or MST, has been developed (Avalosse and Rubin, 1999). This robust technique greatly simplifies the meshing of the geometric entities and does not present the complexities and limitations of other commonly used techniques. The transient algorithm was

112

developed for two-dimensional and three-dimensional non-isothermal, generalized Newtonian fluids. It is designed to work with a finite element solver. A mesh is generated for each part of the flow simulation: one for the flow domain and one for each screw. The screws are assumed to be rigid and their motion is a combination of translation and rotation. At each timestep the screw meshes are moved to a new position, overlapping the flow mesh. For each node of this new domain that lies within a given screw, a special formulation is used that imposes a velocity that matches the rotation speed of the screw. The movement of the screws imparts momentum to the surrounding fluid. The flow is calculated in this manner for a set of successive screw positions at constant angular displacement. The history of the flow pattern is thus obtained and stored for further analysis.

Figure 30.1 shows the grid for a typical twin-screw extruder. The grid in the screw regions is shown on the surfaces of the elements.
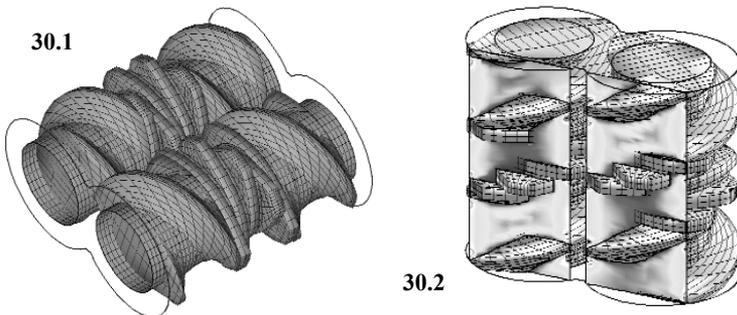
Figure 30
The mesh superposition technique was used to model the complex, time-dependent flow in a twin-screw extruder. The flow of polystyrene was analyzed throughout a combination of conveying and kneading block elements. The surface grid for the screws is shown in Figure 30.1. The figure on the right (30.2) shows the local shear rate on a planar slice through the twin-screw extruder, with white denoting regions of high shear rate and black denoting regions of low shear rate. Three meshes were used for this configuration, one for each screw and one for the flow domain.

113

The black lines show the outline of the region containing the fluid. Figure 30.2 shows the shear rate on a planar surface through the extruder. High shear rates are found near the tips of the extruder elements, as expected. This information is relevant when dealing with shear sensitive materials.

Other quantities of interest, such as residence time distributions, material thermal history, and stretching rates, for example, can also be obtained. This allows for a detailed comparison between alternative designs. For example, using this technique it was found that an extruder in which conveying elements were alternated with kneading elements provided 25% better mixing per unit length than a standard extruder that contained only conveying elements. The residence time distribution was narrower, however, with the standard design. Being able to obtain such detailed performance information without experimentation allows process engineers to design advanced and more efficient process equipment with confidence.

7.9 Intermeshing Impellers

The mesh superposition technique (MST) can also be used to model the flow in vessels equipped with multiple impellers whose swept volumes overlap. In this example, the mixing in such a system operating at a very low Reynolds number (1×10^{-4}) is considered. Figure 31 shows two anchor impellers mounted on separate shafts. The impellers are set at a 90° angle relative to each other. Although the impellers do not touch each other, there is a volume that is swept by both impellers. Such a system cannot be modeled using the sliding mesh models implemented in most commercial CFD programs. The main benefits of using the mesh superposition technique for such as system are that each

part can be meshed separately, and that these intermeshing parts can rotate freely without having to be remeshed.

| t = 0 | 1-3/4 rotations | 2-1/8 rotations | 6 rotations |
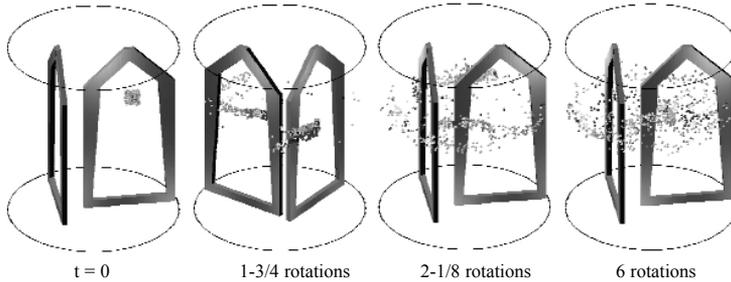
Figure 31
The dispersion of a particle tracer in a vessel equipped with two intermeshing anchor impellers as calculated using the mesh superposition technique. After six full rotations, the particles are well dispersed on the horizontal plane where they were released.

To create the mixer geometry, a cylindrical mesh is generated for the tank. Two other, completely independent meshes are defined for the blades. The three meshes are then combined into one. As the blades rotate, the transient flow pattern in the tank can be calculated, and illustrated by the dispersion of tracer particles, as shown in the figure. As the total number of rotations increases, the tracer becomes more uniformly distributed. After six rotations, the dispersion of the tracer particles in the horizontal plane is satisfactory. Note, however, that the particles have moved little in the vertical direction. This is because the anchor impellers in use impart little or no axial momentum to the fluid. Twisted blades, which also impose and axial motion on the flow, might perform better to distribute the tracer throughout the vessel. The mesh superposition technique is well suited to study such systems.

7.10 Kenics Static Mixer

Static mixers are widely used in the process industries. Static

mixers consist of motionless elements mounted in a pipe, which create flow patterns that cause fluids to mix as they are pumped through the pipeline. Most of the experimental work on static mixers has concentrated on establishing design guidelines and pressure drop correlations. The number of investigations into the flow and mixing mechanisms is limited, probably due to difficulties encountered in obtaining meaningful experimental measurements.

The Kenics in-line mixer consists of a number of elements of alternating right- and left-hand 180-degree helices. The elements are positioned such that the leading edge of each element is per-pendicular to the trailing edge of the previous element. The length of the elements is typically one and a half tube diameters. This type of static mixer is used for mixing under laminar flow conditions, such as the mixing of polymers or food products, like peanut butter and chocolate.

To evaluate the mixing mechanism of the Kenics mixer, Bakker and Marshall (1992) and Bakker and LaRoche (1993) calculated the transport of two chemical species through a six-element device. The center of the inlet was 100% of one species, desig-nated by white in Figure 32. The outside of the inlet was 100% of the other species, shown as black. The results are presented as a series of contour plots, showing the concentration fields of the chemical species at various axial positions along the tubes. The concentration fields after 18, 54, 90, 126, and 162 degrees of rotation in each of the six Kenics mixing elements are shown. In the first element, the white core coming from the inlet is split into two white islands. These islands are stretched and move outward. The black, which was initially on the outside, is split into two semi-circular filaments, which move towards the inside. Similar stretching and folding processes occur in the next several elements.

116
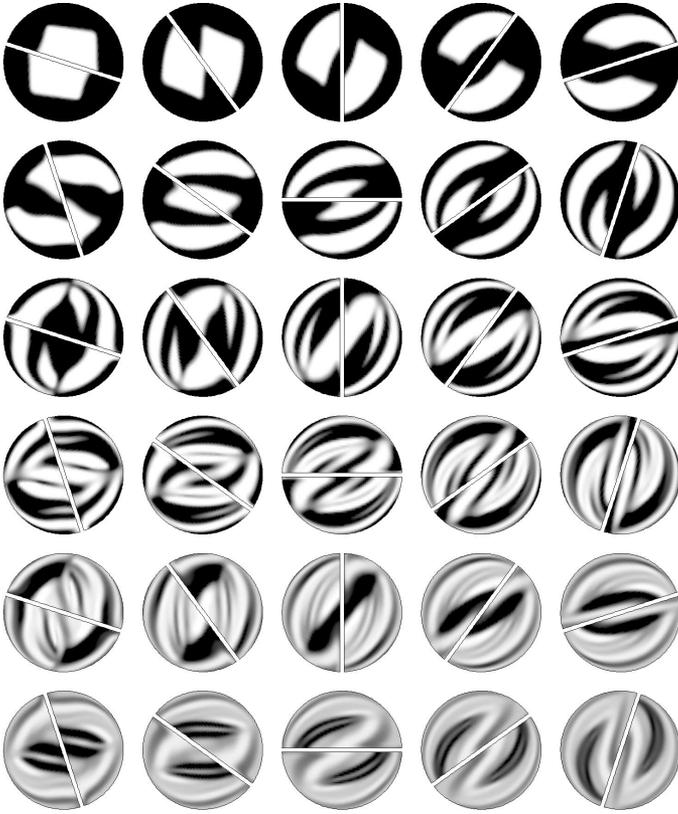
Figure 32
Concentration profiles in the mixer. Rows one to six show the concentration in elements one to six respectively. Columns one to five show the concentration profiles at 18°, 54°, 90°, 126°, and 162°, respectively.

At the inlet of the third element the black species is now on the inside, meaning that the concentration field has basically flipped inside out. This process of splitting, stretching, folding and flipping inside out repeats itself every two elements, until the fluids are mixed. The number of elements can be adjusted to the requirements of the process, but typically varies between six and eighteen depending on the Reynolds number.

117

7.11 HEV Static Mixer

The traditional helical mixing element is mainly used for in-line blending under laminar and transitional flow conditions. The High Efficiency Vortex (Chemineer HEV) mixer is used for turbulent blending of gases or miscible liquids. It consists of a series of tab arrays, which are placed along a length of pipe. The advantages of this design are that it is easily adapted to both cylindrical and square pipe cross-sections, and that it has a relatively low pressure drop. HEV mixers have been in use in the process industries for several years now, both for liquid-liquid and gas-gas mixing. Applications include waste-water treatment, burners, exhaust stacks, beverage manufacturing, and many others. The wide range of applications and scales in which the HEV mixer is used requires a technique to analyze custom applications on demand. Gretta (1990) investigated the flow pattern generated by the tabs using a combination of hot wire anemometry, hydrogen bubble visualization and dye visualization, and found that the tabs not only generate a pair of counter-rotating, longitudinal vortices but also shed so-called hairpin vortices. The smaller hairpin vortices, generated in a transient manner, move downstream with the larger longitudinal vortices.

Bakker *et al.* (1994) modeled the flow pattern generated by an HEV mixer using the Reynolds stress model for turbulence. This steady-state model correctly predicted the formation of the longitudinal vortices, but the hairpin vortices only showed up in the results as regions of high turbulence intensity at the edges of the tabs. Due to the steady-state nature of that model and the assumption of eight-fold symmetry made for the purpose of the calculation, the mixing of fluids near the center of the pipe was underpredicted compared to what was known from operational experience and laboratory studies.

Because of the shortcomings of the RANS turbulence models in predicting the hairpin vortices, the HEV mixer was selected as a good candidate for the LES turbulence model. In the LES model, no symmetry assumptions were made, meaning that the full 360° pipe was modeled. The advantage of modeling the full pipe is that periodic interactions between the vortices that form behind the different tabs are not restrained. The simulation was started with a steady-state calculation based on the k-ε turbulence model. After partial convergence, the LES model was enabled. As expected, the transient results showed the periodic shedding of hairpin vortices off the back sides of the tabs. Figure 33 shows these vortices at two different instances in time. It is clear that the hairpin vortex forming around the tab on the left has shifted downstream during the 0.06 s that separates the two flow pattern snapshots. This shows that the LES model is well suited to capture complex, time dependent vortex systems such as these.
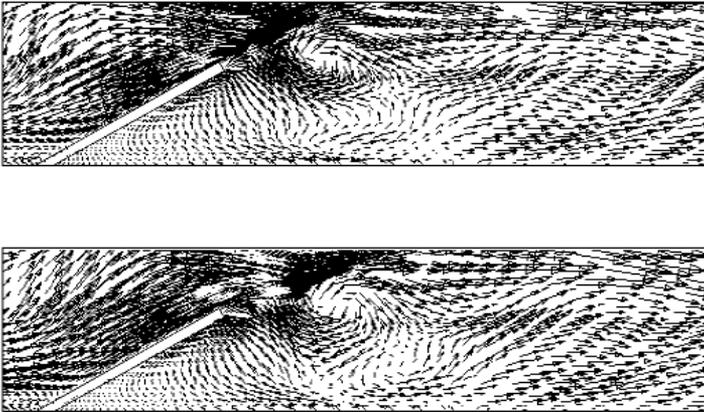
Figure 33
This image shows the hairpin vortex (in cross-section) that forms behind the tab in an HEV mixer at two different instances in time. Vortices such as these are shed in a time dependent fashion. The LES model was used for this simulation. A similar HEV mixer, solved using the steady-state Reynolds stress turbulence model, failed to capture this flow detail.

119

COMPUTATIONAL FLUID MIXING

7.12 LDPE Autoclave Reactor

Low density polyethylene (LDPE) reactors are used to manufacture polymer products. The reactors are typically of the tubular or autoclave variety. To make the (multi-molecule chain) polymer, a minute amount of initiator is added to a (single-molecule) monomer. Several reaction steps take place in which the monomer is transformed to intermediate polymers, or radicals, and finally to a polymer product with a range of chain lengths (corresponding to a range of molecular weights). Heat is released in many of the reactions, and one goal of LDPE reactor design is to prevent hot spots that give rise to a condition called thermal runaway, which is characterized by an undesired product distribution.

In this example, the nearly infinite set of reactions in the chain is approximated by six finite-rate reactions using the method of moments (Kiparissides *et al.* (1997)). These reactions are solved using the finite rate reaction model with the help of user-defined functions. As a consequence of the method of moments, quantities that describe the product distribution can also be computed. These include the molecular weight distribution, which, if narrow, indicates a high quality (uniform) product.

A hybrid mesh of 166,000 cells, shown in Figure 34, is used for the simulation. The reactor contains both paddle and twisted blade impellers, whose rotation is modeled using a sliding mesh. The monomer and initiator used are ethylene and DTBP, respectively. The initiator is pre-mixed with the monomer and injected into the reactor through an annular ring at one end of the vessel. The mixture leaves the device through an annular exit at the opposite end. The flow field is characterized by high swirl, which is induced by the rapidly rotating impellers in the unbaf-

fled vessel. The RNG k-ε model is used to account for turbulence in the highly swirling flow.
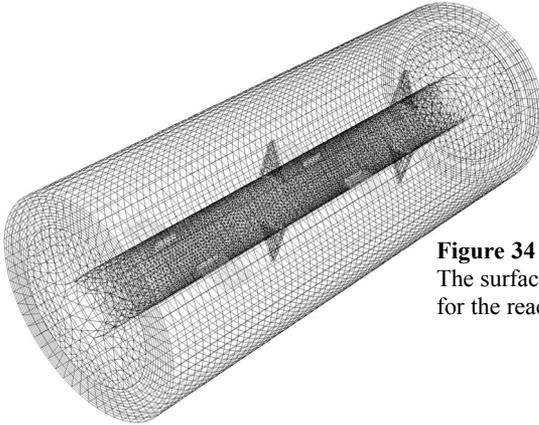
Figure 34
The surface mesh used for the reactor.

Four axial slices are used in the next two figures to show the progression of two problem variables as the mixture advances through the reactor. In these figures, the inlet annulus is at the top of the figure and the outflow annulus is at the bottom. In Figure 35 the conversion of the monomer (to both radicals and product polymers) is shown to gradually increase to about 7% as the flow passes through the vessel, in reasonably good agreement with published data (Read *et al.* (1997)). Contours of the molecular weight distribution (Figure 36) vary from 41,500 to 41,900, or by about 1%. As the mixture moves through the reactor, the spread in the distribution narrows, indicating a product of high quality. The solution also indicates that the molecular viscosity increases as the chains of radicals grow, consistent with expectations.

Figure 35
The conversion of monomer increases to about 7% as the material moves through the reactor. The flow is from top to bottom. The darker color of the bottom indicates a higher conversion rate.

Figure 36
Contours of molecular weight distribution are used to assess the range of molecular weights in the product. The range is narrower near the exit at the bottom of the reactor than near the inlet at the top.

7.13 Impeller Design Optimization

Ever since the 1950s the Rushton turbine has been the standard impeller for gas dispersion applications. It features six flat blades mounted on a disk. As shown in Figure 20.2, the flow behind the impeller blades separates, and trailing vortices form. On gassing, gas accumulates in the low-pressure regions behind the blades and cavities form. This leads to a significant drop in power draw

and loss of gas dispersion ability. During the late 1980s and early 1990s, modified Rushton turbines with semi-circular blades became standard. These models reduce flow separation and cavity formation behind the blades, but do not eliminate them completely.

To date, the disk-style gas dispersion impellers studied in the literature have blades that are symmetric with respect to the plane of the disk. This is not necessarily optimal, since the gas usually enters from the bottom, causing a distinctly asymmetric flow pattern. In this example, the operation of the Chemineer BT-6 gas dispersion impeller is reviewed [Bakker (1998) and Myers *et al.* (1999)]. The BT-6 impeller, with vertically asymmetric blades, is designed to accommodate the different flow conditions above and below the impeller disk.

The turbulent flow pattern created by the BT-6 was modeled using a fully unstructured tetrahedral mesh with approximately 500,000 cells. The MRF approach and RNG k-ε turbulence model were used. Second order upwind differencing was used for the momentum and turbulence equations. The flow pattern was converged using the SIMPLEC pressure-velocity coupling method, which allows for the use of high underrelaxation factors, resulting in fast convergence.

The triangular mesh on the impeller blade is shown in Figure 37. The blades have a concave shape, which consists of three curves of different radii and length. The top part of the blade is longer than the bottom part. The backside of the blade is rounded.

After the flow field was converged, the torque on the impeller was calculated by integrating the pressure on the impeller blade

surfaces. From the torque, the impeller power number, based on the nominal diameter at the impeller disk level, was calculated to be 2.3, which is in excellent agreement with experiments.
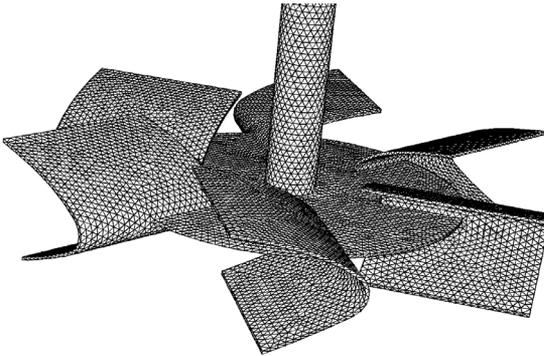
Figure 37
The triangular surface mesh on a BT-6 impeller.

Figure 38 shows the velocity field around the impeller blades. The velocity vectors are drawn in the frame of reference of the impeller. It is clear that no flow separation behind the impeller blades occurs. This means that cavity formation under gassed conditions will be reduced. Indeed, visualization studies have shown that gas is captured under the top overhang and dispersed from a deep vortex on the inside of the blade. No large gas-filled cavities have been observed behind the blade. As a result, the BT-6
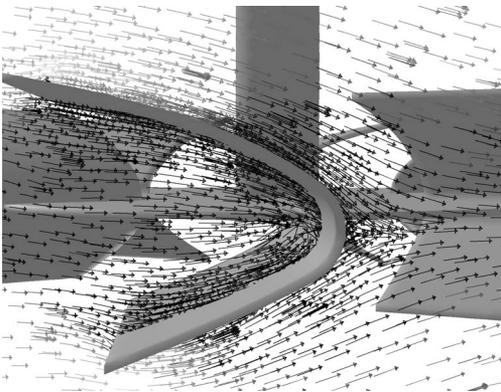
Figure 38
Velocity field around the blades of a BT-6 impeller. No flow separation occurs behind the blades.

has a gassed power curve that is flatter than that of other impellers. It can disperse more gas before flooding than the impellers with symmetric semi-circular blades, and is less affected by changes in liquid viscosity.

7.14 Helical Ribbon Impeller

High-viscosity mixing applications occur in most chemical process industry plants. For instance, the polymer industries must blend high-viscosity reaction masses to thermal and chemical uniformity. This industry must also blend small amounts of low-viscosity antioxidants and colorants into polymer streams. The personal-care products industry encounters many high-viscosity mixing applications in the preparation of creams, lotions, pastes and drugs. Other high-viscosity applications occur in the production of food, paint, drilling mud, and greases, to name a few. Viscosities can be in the range from about one Pa-s all the way up to 25,000 Pa-s in some extreme cases. The quality of the final mixed product in these applications can be very important economically.

Low-viscosity mixing applications can usually be handled efficiently with impeller systems consisting of one or more turbines. To obtain adequate mixing under the laminar flow conditions encountered in high viscosity applications, on the other hand, close-clearance impellers such as anchors and helical ribbons are required. These impellers sweep the whole wall surface of the vessel, and agitate most of the fluid batch through physical contact. Helical ribbon impellers are typically used for industrial applications where the viscosity is in the range of 20 to 25,000 Pa-s. Wall scrapers can be mounted on the impeller blades to improve heat transfer.

Figure 39 shows the flow pattern in the vertical plane of a vessel equipped with a helical ribbon. A fully structured hexahedral mesh with approximately 100,000 cells was used. The structured 3-D mesh was created by extruding and twisting a 2-D planar mesh. The fluid is viscous and the impeller Reynolds number is approximately 10. The velocity vectors show that the impeller pumps down at the wall and up in the center. Contours of velocity magnitude on the tank bottom show that there are low velocities in the center and higher velocities near the outside wall. Small circulation loops form between the impeller blades and the vessel wall, as discussed in the general literature. These indicate the need for an even larger D/T or the use of wall scrapers if optimum heat transfer is to be obtained.
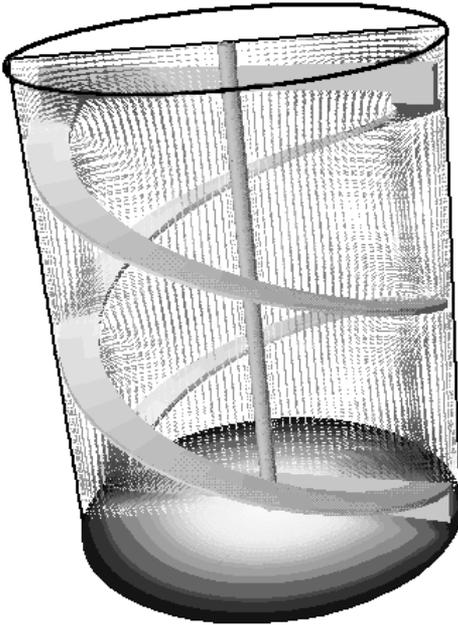
Figure 39
The flowfield in a vessel equipped with a helical ribbon impeller. Velocity vectors in a vertical plane are shown. The bottom of the vessel is colored by velocity magnitude.

7.15 Stirred Tank Modeling Using LES

In turbulent flows, large-scale eddies with coherent structures are primarily responsible for the mixing of passive scalars. The large-scale eddies embody themselves in the form of identifiable and organized distributions of vorticity. In addition, the mixing process involves all mechanisms typically found in vortex dynamics, such as stretching, break-up, concatenation, and self-induction of vortices.

Recent experimental work suggests that large-scale, time-dependent structures, with periods much longer than the time of an impeller revolution, are involved in many of the fundamental hydrodynamic processes in stirred vessels. For example, local velocity data histograms may be bi-modal or tri-modal, even though they are being analyzed as having only one mode in most Laser-Doppler experiments. In solids suspension processes, solids can be swept from one side of the vessel to the other in an oscillating pattern, even in dilute suspensions. Digital particle image velocimetry experiments have shown that large-scale asymmetries with periods of up to several minutes exist in stirred vessels equipped with axial flow impellers.

The advantage of Large Eddy Simulation (LES) over other turbulence models is that it explicitly resolves the large eddies, which are responsible for much of the mass, energy, and momentum transport. Only the small eddies are represented by a time-averaged sub-grid scale model. In mixing tank simulations, the LES turbulence model is typically combined with a sliding mesh model for the impeller so that the most rigorous time-accurate solution can be obtained.

COMPUTATIONAL FLUID MIXING

One parameter that is pivotal to the success of an LES simulation is the density of the grid throughout the domain. To determine an optimum grid size, the following, straightforward method is recommended. First a steady-state, three-dimensional calculation is performed that uses the standard k-ε turbulence model and the MRF model for the impeller. From the converged flow field, volume averages for the following three turbulent length scales are calculated:

· Integral length scale: $L_t = k^{3/2}/\varepsilon$
· Taylor length scale: $L_a = (15\nu u'^2/\varepsilon)^{0.5}$
· Kolmogorov scale: $L_k = (\nu^3/\varepsilon)^{1/4}$

The integral length scale is a measure of the large-scale turbulence. The Kolmogorov length scale is a measure of the smallest scale eddies at which dissipation occurs. The Taylor length scale is an intermediate length scale that can be used as a guide to determine the grid size required for an LES simulation. For a typical turbulent small-scale vessel, $L_t/T \sim 10^{-1}$, $L_a/T \sim 10^{-2}$, and $L_k/T \sim 10^{-3}$. Based on the Taylor length scale, a suitable grid size for an LES simulation would be on the order of 10^{-2} T, which would result in a grid on the order of 10^6 cells. The large number of cells along with the transient solution method (one that requires a small time-step), contribute to the increased calculation time required by the LES model when compared to RANS models. Figure 40 shows how the CPU time and required grid size for the LES model compare with other turbulence modeling options.

In this example, the use of LES and the sliding mesh model to predict large-scale chaotic structures in stirred tanks is demonstrated for a single high-efficiency impeller. A full hexahedral mesh was used for the simulation. The vessel diameter is 0.29 m,

128
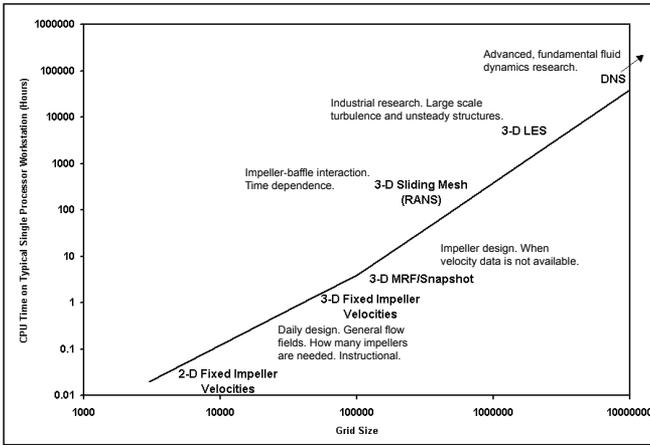
Figure 40
The CPU time and grid size requirements for various impeller modeling options.
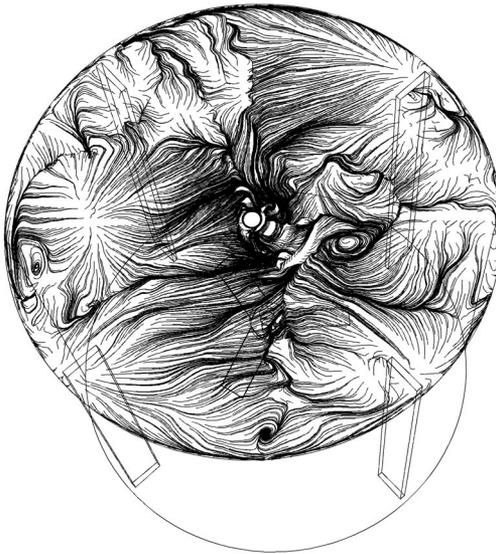
Figure 41
The flow pattern at the surface of a vessel equipped with a high-efficiency impeller as calculated using the LES turbulence model.

and the impeller rotates at 60 RPM, resulting in a Reynolds number of 13,000. The central differencing scheme for the momentum equations was used along with a time step of 0.01 s. The

129

COMPUTATIONAL FLUID MIXING

RNG modification of the Smagorinsky model was used for the sub-grid scale turbulence. A period of approximately 40 seconds was simulated. The results show that the flow pattern indeed exhibits large-scale unsteady motion, similar to what has been reported from experimental data in the literature. Figure 41 shows the flow field at the liquid surface at one instant in time, using oilflow lines, which are pathlines that are confined to the surface from which the flow followers are released. The turbulent structure of the flow is clearly visible.

When performing such LES calculations, it is advised to visualize the results by creating flow field images after every time step. These can then be used to create animations. Similarly, statistical data can be obtained by creating monitor points or lines in the domain and saving important variables in these locations. The time series that are obtained in this manner can be further analyzed using standard statistical and signal analysis techniques.

VIII

CLOSING REMARKS

It could be said that what comes out of a CFD simulation is only as good as what goes in. While this is true in part, there are many other considerations that can lead to the success - or lack thereof - of CFD. One is based on the choice of software. Many commercial packages are available today, and resources to help find and evaluate them are given in Section 8.1. Comments on basic hardware requirements for CFD codes, which are computationally intensive, are found in Section 8.2. Issues regarding the learning curve, or the time required for an engineer to "come up to speed" and be successful with CFD, are discussed in Section 8.3. Once the proper software, proper hardware, and trained user are in place, there are still some common pitfalls to be avoided. These, along with some of the benefits of CFD, are discussed in Section 8.4.

8.1 Additional Resources
Many commercial, and even some freeware or shareware CFD codes are available, each with different capabilities, special physical models, numerical methods, geometric flexibility, and user interfaces. Specialized pre- and post-processing programs are

also available for the generation of the geometry and grid, input of model parameters, and viewing of results. Excellent overviews of these products can be found on the web. See, for example, CFD Review (Wyman). The increased use of CFD in the chemical industries has led to the formation of a dedicated chemical process CFD user group (LaRoche), which provides another excellent resource for the mixing analyst.

8.2 Hardware Needs

In the past, CFD usage was often associated with the realm of high-powered computer systems. But much of today's modeling work can be accomplished on low-end Unix workstations, or high end PCs. A typical PC configuration might be a one or two-processor system, running Windows or Linux. Unix workstations with one, two, or more processors are also commonly used. These systems are more than adequate for moderately-sized, steady state or time-dependent analyses. For complicated models, or those using a large number of computational cells (> 1 million), multi-processor workstations are often used. Although super-computers are still employed for high-end research and development work, they are not commonly needed for typical engineering design applications. Another recent trend involves the clustering of multiple inexpensive PCs into a parallel-, or cluster-computing network. Such systems provide supercomputing power at a fraction of the cost.

8.3 The Learning Curve

The user-friendliness of CFD software has also increased significantly during recent years. In the past, CFD software was characterized by text- or command-file based interfaces and difficult to configure solvers, that made fluid flow analysis the exclusive

domain of highly trained experts. However, the latest generation of commercial CFD software has been developed with graphical user interfaces. They have much more stable and robust solvers, and allow easy geometry exchange between CAD programs and the CFD solver. This has allowed engineers who are not experts in fluid dynamics to make efficient use of CFD and use this technology on a day-to-day basis in their design and optimization work. Most commercial CFD companies provide training and ongoing technical support with a software license. The average engineer typically requires one week of training to get started using one of these modern CFD packages.

8.4 Common Pitfalls and Benefits

Despite the increased user-friendliness of modern CFD software, there are still a number of potential pitfalls that can beset the analyst. Some of the most commonly made mistakes when using CFD are listed below.

- **Use of a low quality, coarse grid**
  Details that are smaller than the cell size cannot be resolved. Often, small flow features in one region need to be resolved in great detail in order to accurately predict large flow features in other regions. For example, a jet penetrating into a vessel will appear to diffuse more rapidly than in actual fact if a coarse grid is used in the jet region. Satisfying grid needs such as this may lead to a finer grid containing far more cells than was initially estimated.
- **Use of unconverged results**
  CFD solvers are iterative and it is often tempting to cut a calculation short when deadlines are approaching or the coffee break is over. However, the analyst should always

ensure that proper convergence has been obtained before using the results from any CFD solver.

· **Use of the wrong physical property data**
  This is not as trivial as it sounds. For example, viscosity curves may have been determined in one temperature and shear rate range, but if the actual shear rates or temperatures in the flow domain are outside of this range the curves may no longer be valid and incorrect results may be obtained. As another example, accurate average particle size and density is needed to best predict solids suspension behavior.

Fortunately, none of these problems is fundamental to the CFD technology itself. A coarse grid may be refined, unconverged calculations continued, and accurate physical constants may be measured. These easily avoided pitfalls are far outweighed by the following benefits:

❑ CFD can be used to augment design correlations and experimental data.

❑ CFD provides comprehensive data that is not easily obtainable from experimental tests.

❑ CFD reduces scale-up problems, because the models are based on fundamental physics and are scale independent. Models of the actual unit can be simulated just as easily as models of lab scale versions, so predictions, and indeed optimization of the actual unit can be achieved.

❑ When evaluating plant problems, CFD can often be used to help understand the root cause of a problem, not just the effect.

❑ CFD can be used to complement physical modeling. Some design engineers actually use CFD to analyze new systems

before deciding which and how many validation tests need to be performed.

❑ Many "what if" scenarios can often be analyzed in less time than experimental tests would take.

In summary, if the CFD analyst is careful when addressing the issues of problem setup and solution convergence, the potential benefits that can be extracted from the simulation are numerous. Furthermore, the computational resources available today, both in terms of speed and power, should encourage engineers to make use of high density grids and complex models so as to achieve results of the best possible quality.

COMPUTATIONAL FLUID MIXING

NOTATION

A	Magnussen mixing rate constant (-)
A_k	Arrhenius constant for reaction k (variable units)
B	Magnussen mixing rate constant (-)
C	Off-bottom clearance (m)
C_1	Turbulence model constant (-)
C_2	Turbulence model constant (-)
C_A	Concentration of species A (mole m^{-3})
c_A	Fluctuation in the concentration of species A (mole m^{-3})
$C_{j'}$	Concentration of species j' (mole m^{-3})
D	Impeller diameter (m)
E	Total enthalpy (J)
E_k	Activation energy for reaction k (J mole^{-1})
f	Underrelaxation factor (-)
$F(\phi)$	Spatially discretized transport equation
F_i	Net force in the i direction (N)
g	Gravitational acceleration (m s^{-2})
G_k	Generation term for turbulence (kg m^{-1} s^{-3})
$J_{i',i}$	Diffusion flux of species i' in direction I (kg m^{-2} s^{-1})
h	Static enthalpy (J)
$h_{j'}$	Enthalpy for the species j' (J)
k	Turbulent kinetic energy (m^2 s^{-2})
k_{eff}	Effective conductivity (W m^{-1} K^{-1})
$K_{i',k}$	Reaction rate of species i' in reaction k (variable units)
L	Length of domain in definite integral over coordinate x (m)
L_a	Taylor length scale (m)
L_k	Kolmogorov scale (m)
L_t	Integral length scale (m)
$m_{i'}$	Mass fraction of species i' (-)
$M_{i'}$	Molecular weight of species i' (kg/kgmole)

COMPUTATIONAL FLUID MIXING

N	Impeller rotational speed (s^{-1})
N_P	Power number (-)
N_Q	Flow number (-)
P	Power drawn by an impeller (W)
p	Pressure (Pa)
Pe	Peclet number (-)
Q_l	Liquid flow rate (m^3 s^{-1})
r	Spatial coordinate in the radial direction (m)
R	Universal gas constant (J mole^{-1} K^{-1})
R	Impeller radius (m)
Re	Reynolds number (-)
$R_{i'}$	Generalized source term for reactions in the species i' transport equation (kg m^{-3} s^{-1})
$R_{K\_i',k}$	Kinetic reaction rate for species i' in reaction k (kg m^{-3} s^{-1})
$R_{M1-i',k}$	Mixing limited reaction rate for the reactant species i' in reaction k (kg m^{-3} s^{-1})
$R_{M2-i',k}$	Mixing limited reaction rate for the product species i' in reaction k (kg m^{-3} s^{-1})
R_P	Residual at the point P
S_h	Generalized source term for the enthalpy equation (W m^{-3})
$S_{i'}$	Net species source term in the species i' transport equation (kg m^{-3} s^{-1})
t	Time (s)
T	Tank diameter (m)
T	Temperature (K)
T_{ref}	Reference temperature for formation enthalpy (K)
U	Velocity vector (m s^{-1})
U_i	Velocity in the direction i (m s^{-1})
u_i'	Fluctuating velocity component (due to turbulence) in the direction i (m s^{-1})
U_{tip}	Impeller tip speed (m s^{-1})

138

W_b	Width of impeller blade (m)
x_i	Spatial coordinate in direction i (m)
X_s	Product distribution (-)
z	Impeller blade height (m)

Greek Symbols

α	Volume fraction of catalyst (-)
β_k	Temperature exponent in Arrhenius rate expression (-)
Γ	Generalized diffusion coefficient (variable units)
δ_{ij}	Kronecker delta (-)
ε	Turbulent kinetic energy dissipation rate (m^2 s^{-3})
$\eta_{j',k}$	Exponent for concentration of species j' in reaction k (-)
ϕ	Generalized conserved quantity (variable units)
μ	Molecular viscosity (kg m^{-1} s^{-1})
μ_{eff}	Effective viscosity (kg m^{-1} s^{-1})
μ_t	Turbulent viscosity (kg m^{-1} s^{-1})
$v_{i'}$	Stoichiometry of species i' (-)
Ω	Angular speed (rad/sec)
ρ	Liquid density (kg m^{-3})
σ_k	Turbulence model constant (-)
σ_ε	Turbulence model constant (-)
σ_μ	Turbulence model constant (-)
τ	Shear stress (Pa)
τ_d	Disruptive shear stress (Pa)
τ_y	Yield stress (Pa)
ξ	Vorticity (s^{-1})

REFERENCES

Avalosse, T., and Y. Rubin, *Analysis Of Mixing In Co-Rotating Twin Screw Extruders Through Numerical Simulation*, 15th Polymer Proc. Society Conference, `s Hertogenbosch, the Netherlands, March 1, 1999.

Bakker, A., *Hydrodynamics of Stirred Gas-Liquid Dispersions*, PhD Thesis, Delft University of Technology, 1992.

Bakker A., *Impeller Assembly with Asymmetric Concave Blades*, US Patent 5791780, 1998.

Bakker A., N. Cathie, and R. LaRoche, *Modeling of the Flow and Mixing in HEV Static Mixers*, 8th European Conference on Mixing, September 21-23, 1994, Cambridge, U.K. IChemE Symposium Series No. 136, ISBN 0 85295 329 1, p. 533-540, 1994.

Bakker A., and J. B. Fasano, *A Computational Study of the Flow Pattern in an Industrial Paper Pulp Chest with a Side Entering Impeller*, Annual AIChE Meeting, November 1992. AIChE Symposium Series 293, Volume 89, 1992, p. 118-124, 1993.

Bakker A., and J. B. Fasano, *Time Dependent, Turbulent Mixing and Chemical Reaction in Stirred Tanks*, Annual AIChE Meeting, November 1993, St. Louis, Missouri. AIChE Symposium Series 299, Volume 90, 1993, p. 71-78, 1993.

Bakker A., J. B. Fasano, and K. J. Myers, *Effects of Flow Pattern on the Solids Distribution in a Stirred Tank*, 8th European Conference on Mixing, Cambridge, U.K. IChemE Symposium Series No. 136, ISBN 0 85295 329 1, p. 1-8, September 21-23, 1994.

Bakker A., A. Haidari, and E. M. Marshall, *Modeling Stirred Vessels Using Large Eddy Simulation*, 18th Biennial North American Mixing Conference, Pocono Manor, PA, June, 2001.

COMPUTATIONAL FLUID MIXING

Bakker A. and R. LaRoche, *Flow and Mixing with Kenics Static Mixers*, Cray Channels, Volume 15, Number 3, p. 25-28, 1993.

Bakker, A., R. D. LaRoche, M. H. Wang, and R. V. Calabrese, *Sliding Mesh Simulation of Laminar Flow in Stirred Reactors*, Trans. IChemE., **75**, Part A, January, 1997.

Bakker A. and E. M. Marshall, *Laminar Mixing with Kenics In-Line Mixers*, Fluent Users Group Meeting Proceedings, p. 126-146, October 13-15, Burlington, Vermont, 1992.

Bakker, A., L. Oshinowo, and E. Marshall, *The Use of Large Eddy Simulation to Study Stirred Vessel Hydrodynamics*, Proceedings of the 10th European Conference on Mixing, Delft, The Netherlands, p. 247 - 254, July 2-5, 2000.

Bakker, A., J. M. Smith, and K. J. Myers, *How to Disperse Gases in Liquids*, Chemical Engineering, Dec., 1994.

Bakker A. and H. E. A. Van den Akker, *Single-Phase Flow in Stirred Reactors*, Chemical Engineering Research and Design, Trans. IchemE **72**, Number A4, p. 583-593, July, 1994.

Bourne, J.R., F. Kozicki, and P. Rys, *Mixing and Fast Chemical Reaction - I; Test Reactions to Determine Segregation*, Chem. Eng. Sci., **36**(10), p. 1643, 1981.

Ding, J., and D. Gidaspow, *A Bubbling Fluidization Model Using Kinetic Theory of Granular Flow*, AIChE J., V. **36**(4), p. 523-538, 1990. FLUENT 5 User's Guide, Fluent Incorporated, 1998.

Fokema, M. D., S. M. Kresta, and P. E. Wood, *Importance of Using the Correct Impeller Boundary Conditions for CFD Simulations of Stirred Tanks*, Canadian J. of Chem. Eng., **72**, p. 177-183, 1994.

REFERENCES

Fox, R. O., *On the Relationship Between Lagrangian Micromixing Models and Computational Fluid Dynamics*, Chem. Eng. and Proc. **37**, p. 521-535, 1998.

Fryer, C., and O.E. Potter, *Experimental Investigation of Models for Fluidized Bed Reactors*, AIChE J. **22**, p. 38-47, 1976.

Gidaspow, D., M. Syamlal, and Y. C. Seo, *Hydrodynamics of Fluidization: Supercomputer Generated vs. Experimental Bubbles*, J. Powder & Bulk Solids Tech. **10** (3), p.19-23, 1986.

Gran, I. R., and B. F. Magnussen. *A Numerical Study of a Bluff-Body Stabilized Diffusion Flame. Part 2. Influence of Combustion Modeling and Finite-Rate Chemistry*, Combustion Science and Technology, p. 119-191, 1996.

Gretta W. J., M.Sc. Thesis, Lehigh University, Bethlehem, Pennsylvania, 1990.

Gullichsen J., *Medium Consistency Processing - Fundamentals*, Bleach Plant Operations/TAPPI Seminar Notes, p. 135-142, 1985.

Hannon, J., *Mixing and Chemical Reaction in Tubular Reactors and Stirred Tanks*, PhD Thesis, Cranfield Institute of Technology, U.K., 1992.

Kiparissides, C., D.S. Achilias, and E. Sidiropoulou, *Dynamical Simulation of Industrial Poly(vinyl chloride) Batch Suspension Polymerization Reactors*, Ind. Eng. Chem. Res. **36**(4): 1253, 1997.

LaRoche, R. D., *Chemical Process CFD User Group*, available at http://www.cpcfd.org.

Leonard, B. P., and S. Mokhtari, *ULTRA-SHARP Nonoscillatory Convection Schemes for High-Speed Steady Multidimensional Flow*, NASA TM 1-2568 (ICOMP-90-12), NASA Lewis Research Center, 1990.

COMPUTATIONAL FLUID MIXING

Luo, J. Y., R. I. Issa, and A. D. Gosman, *Prediction of Impeller Induced Flows in Mixing Vessels Using Multiple Frames of Reference*, IChemE Symposium Series No. 136, p.549-556, 1994.

Magnussen, B. F., and B. H. Hjertager, *On Mathematical Models of Turbulent Combustion with Special Emphasis on Soot Formation and Combustion*, In 16th Symp. (Int'l.) on Combustion, The Combustion Institute, 1976.

Marshall, E. M., Y. Tayalia, L. Oshinowo, and R. Weetman, *Comparison of Turbulence Models in CFD Predictions of Flow Number and Power Draw in Stirred Tanks*, Presented at Mixing XVII, Banff, Alberta, Canada, August 15-20, 1999.

Middleton, J.C., F. Pierce, and P. M. Lynch, *Computations of Flow Fields and Complex Reaction Yield in Turbulent Stirred Reactors and Comparison with Experimental Data*, Chem. Eng. Res. Des. **64**, p. 18-21, January 1986.

Myers K.J., A.J Thomas., A. Bakker, and M.F. Reeder, *Performance of a Gas Dispersion Impeller with Vertically Asymmetric Blades*, Trans IchemE **77**, Part A, November 1999, p. 728-730, 1999.

Ogawa, S., A. Umemura, and N. Oshima, *On the Equation of Fully Fluidized Granular Materials*, J. Appl. Math. Phys. **31**, p.483, 1980.

Oldshue, J. Y., and N. R. Herbst, *A Guide to Fluid Mixing*, LIGHTNIN, Rochester, NY 14611, 1992.

Oshinowo L., A. Bakker, and E. M. Marshall, *Mixing Time - A CFD Approach*, Presented at Mixing XVII, Banff, Alberta, Canada, August 15-20, 1999.

Oshinowo L. M., E. M. Marshall, A. Bakker, and A. Haidari, *Benefits of CFD in Modeling Solids Suspension in Stirred Vessels*, Presentation at Session 174: Computational Fluid Mixing. AIChE Annual Meeting. Los Angeles, California, November 12-17, 2000.

144

REFERENCES

Patankar, S. V., *Numerical Heat Transfer and Fluid Flow*, Hemisphere, Washington, DC, 1980.

Ranade, V. V., and S. M. S. Dommeti, *Computational Snapshot of Flow Generated by Axial Impellers in Baffled Stirred Vessels*, Trans I Chem E. **74**, Part A, May, 1996.

Read, N. K., S. X. Zhang, and W. H. Ray, *Simulations of a LDPE Reactor Using Computational Fluid Dynamics*, AIChE Journal **43**(1), p. 104-117, 1997.

Roussinova, V. T., B. Grgic, and S. M. Kresta, *Study of Macro-Instabilities in Stirred Tanks Using a Velocity Decomposition Technique*, Chemical Engineering Research & Design **78** (7), p. 1040-1052, 2000.

Sanyal, J., S. Vasquez, S. Roy, and M. Dudukovic, *Numerical Simulation of Gas-Liquid Dynamics in Cylindrical Bubble Column Reactors*, Chem. Eng. Sci. **54**, p. 5071-5083, 1999.

Shih, T.-H., W. W. Liou, A. Shabbir, and J. Zhu, *A New k-ε Eddy-Viscosity Model for High Reynolds Number Turbulent Flows - Model Development and Validation*, Computers Fluids, **24** (3), p. 227-238, 1995.

Syamlal, M., W. Rogers, and T. J. O'Brien, *MIFX Documentation: Volume 1, Theory Guide*, DOE/METC-9411004, NTIS/DE9400087, National Technical Information Service, Springfield, VA, 1993.

Tipnis, S. K., W. R. Penney, J. B. Fasano, *An Experimental Investigation to Determine a Scale-Up Method for Fast Competitive Parallel Reactions in Agitated Vessels*, AIChE Annual Meeting, St. Louis, MO, November 1993.

Vasquez, S. and V. Ivanov, *A Phase Coupled Method for Solving Multiphase Problems on Unstructured Meshes*, Proceedings of ASME FEDSM 2000: ASME 2000 Fluids Engineering Division Summer Meeting, Boston, Massachusetts, June 11-15, 2000.

COMPUTATIONAL FLUID MIXING

Versteeg, H. K., and W. Malalasekera, *An Introduction to Computational Fluid Dynamics: The Finite Volume Method*, Longman Scientific & Technical, Essex, UK, 1995.

Weetman, R. J., *Automated Sliding Mesh CFD Computations for Fluidfoil Impellers*, 9th European Conference on Mixing, Paris, FRANCE, March, 1997.

Wyman, N., *CFD Review*, available at http://www.cfdreview.com.

Yakhot, V. and S. A. Orszag, *Renormalization Group Analysis of Turbulence: I. Basic Theory*, Journal of Scientific Computing, **1**(1), p. 1-51, 1986.

INDEX

COMPUTATIONAL FLUID MIXING

COMPUTATIONAL FLUID MIXING

NOTES

NOTES